Theory of Nuclear Systems – 2023--2025

- **Results:**

283** articles in peer-reviewed journals **(PRL, PLB, PRC, EPJ A, PRB, PRE, PRA, PRD, Nucl.Phys. A, EPJ Plus, EPJ A, EPJ D, JETP Lett., ЯФ, Physica A, China Phys. C, Particles, IJMPE, J.Phys.G, Molecular Phys., Phys. Chem. Chem. Phys., Phys.Part.Nucl.-17, ….)

- ***Teaching :***

Lectures at Uni. Dubna, UC JINR, TPU, TSU, MPTI, MSU

Supervision of PhD students and students: 15

Defense of dissertations:

Habilitation- 4

65 researchers

Approximately 10 students from member countries, South Africa, and China come annually for internships.

PROJECTS

Microscopic models for exotic nuclei and nuclear astrophysics - 16

Low-energy nuclear dynamics and properties of nuclear systems - 24

Quantum few-body systems - 15

Relativistic nuclear dynamics and nonlinear quantum processes -10

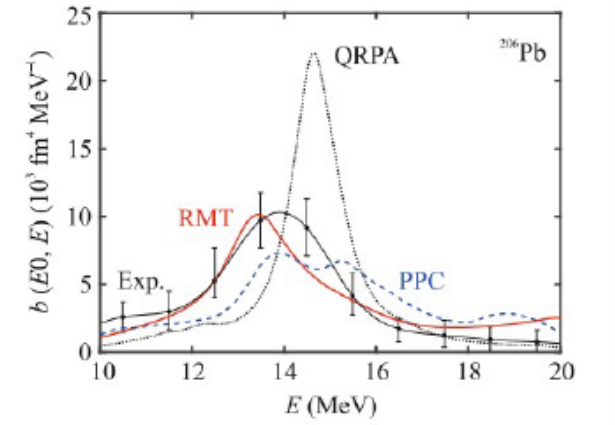

Fig. 5. (Color online) The monopole transition strength $b(E0, E)$ versus the transition energy E in the case of ^{206}Pb. The results, obtained by means of: i) the two-scale RMT approach are connected by (red) solid line; ii) the microscopic PPC calculations are connected by (blue) dashed line; iii) the QRPA approach are connected by (black) dotted line. For a comparison the experimental data [43] shown by (black) squares with error bars, smoothly interpolated, are connected by (black) thin line

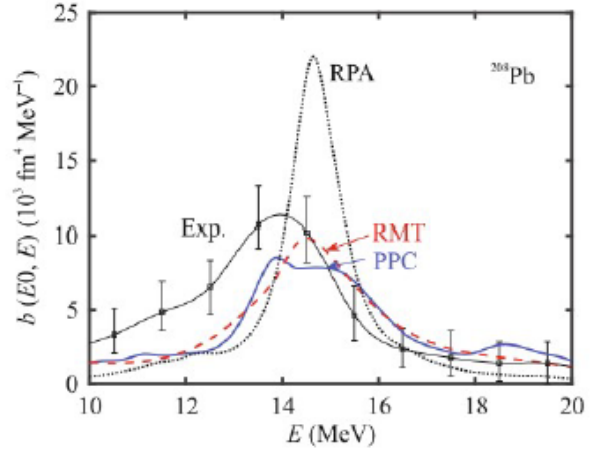

Fig. 7. (Color online) Similar to Fig. 5 but for ^{208}Pb. The RMT results are connected by dashed (red) line, while the PPC results are connected by solid (blue) line

N.N. Arsenyev, A.P. Severyukhin, R.G. Nazmitdinov, "Spreading widths of giant monopole resonance in the lead region: Random matrix approach", JETP Letters 18 (2023) 721 – 722

The gross structure of the strength distribution of giant monopole resonances in nuclei in the vicinity of the doubly magic ^{208}Pb nucleus is described in a good agreement with the experimental data using the idea of a random coupling strength between one- and two-phonon states. One-phonon states are generated by means of the QRPA calculations based on the Skyrme density functional, while the coupling matrix elements between the one-phonon and two-phonon states are replaced by random matrix elements of the Gaussian Orthogonal Ensemble type.

The spreading width of the GMR is described by means of a random matrix approach on two energy scales. It is demonstrated that the main contribution into the decay of the GMR is determined by a small number of two-phonon states strongly coupled to low-energy surface vibrations. While a vast majority of the coupling matrix elements (that are small in value and following the GOE distribution) are responsible for the fine structure of the GMR spreading width.

The remarkable agreement between the results of the PPC and the RMT calculations for the GMR strength distribution of ^{204,206,208}Pb confirms the vitality and validity of the approach. Noteworthy is the fact that the approach can be readily extended to take into account the mixing with three-phonon states.

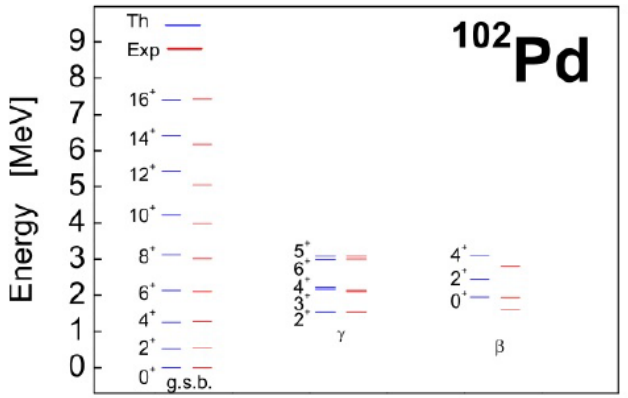

Fig. 1. (color online) Comparison of the excitation energies of ground, γ, and β bands in ^{102}Pd with those obtained via experiment.

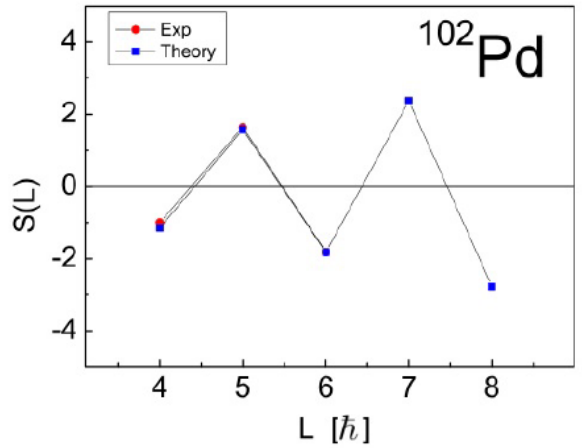

Fig. 4. (color online) Comparison of the experimental and theoretical staggering function $S(L)$ (42) for the states of the γ band in ^{102}Pd.

H. G. Ganev, "Microscopic shell-model description of irrotational-flow dynamics in ^{102}Pd", Ch. Phys. C48 (2024) 014102
"Proton-neutron symplectic model description of ^{106}Cd", Ch. Phys. C48 (2024) 034108

The structure of the low-lying collective excitations in weakly deformed ^{102}Pd and ^{106}Cd was studied within the recently proposed microscopic shell-model version of the Bohr-Mottelson collective model.

For ^{102}Pd, a good description of the excitation energies of the lowest ground, γ, and β bands, as well as the staggering function between the collective states of the γ band and some other energy-dependent quantities, is obtained. The low-energy irrotational-flow quadrupole dynamics is reasonably well described within the present proton-neutron symplectic based shell-model approach without the use of an effective charge.

A good description of the excitation energies of the lowest ground, γ, and β quasibands is obtained for ^{106}Cd without the involvement of adjustable kinetic energy term. The γ degrees of freedom are shown to play a crucial role in the description of spectroscopy of this nucleus. The present approach allows also to describe the observed quadrupole collectivity without the use of an effective charge.

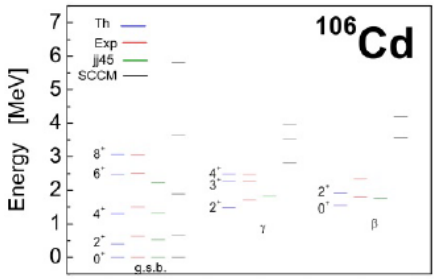

Fig. 1. (color online) Comparison of the excitation energies of the ground, γ, and β quasibands in ^{106}Cd with experiment and predictions of the "jj45" shell-model (extracted from [21]) and the SCCM approach (extracted from [20]). Values of the model parameters (in MeV) are: $B = -0.075$, $C = 0.00045$,

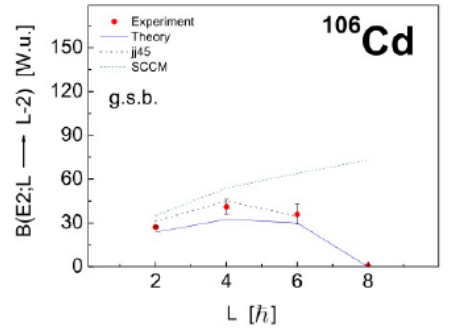

Fig. 2. (color online) Comparison of the experimental [20, 21, 85] and theoretical intraband $B(E2)$ values in Weisskopf units between the states of the ground band in ^{106}Cd. Theoretical predictions of the SCCM approach (SCCM) and the "jj45" shell-model (jj45) calculations (taken from [20] and [21], re-

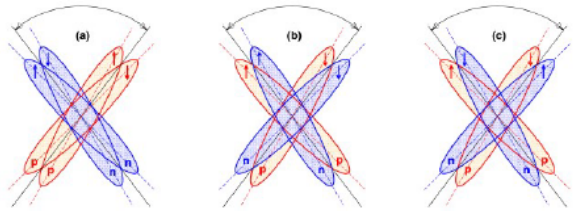

Table 2 The results of WFM calculations for transuranium elements E_i and $B_i(M1)$ are energies (in MeV) and $M1$ strengths (in μ_N^2) of three ($i = 1, 2, 3$) scissors states. $\bar{E}$ is the energy centroid and $\sum B(M1)$ i the summed $M1$ strength

Nuclei	δ	i	E_i	$B_i(M1)$	$\bar{E}$	$\sum B(M1$
		1	1.77	3.10		
$^{238}_{94}$Pu	0.271	2	2.58	5.33	2.52	11.46
		3	3.18	3.03		
		1	1.76	3.10		
$^{240}_{94}$Pu	0.274	2	2.61	5.69	2.55	11.95
		3	3.21	3.16		
		1	1.76	3.09		
$^{242}_{94}$Pu	0.276	2	2.64	6.02	2.58	12.40
		3	3.24	3.29		
		1	1.74	3.05		
$^{244}_{94}$Pu	0.277	2	2.66	6.29	2.60	12.71
		3	3.26	3.37		
		1	1.82	3.38		
$^{240}_{96}$Cm	0.281	2	2.62	5.71	2.57	12.47
		3	3.33	3.38		
		1	1.79	3.29		
$^{244}_{96}$Cm	0.281	2	2.65	6.18	2.59	12.93
		3	3.24	3.46		
		1	1.78	3.25		
$^{246}_{96}$Cm	0.282	2	2.66	6.44	2.61	13.22
		3	3.26	3.54		
		1	1.76	3.18		
$^{248}_{96}$Cm	0.281	2	2.67	6.59	2.61	13.31
		3	3.26	3.55		
		1	1.78	3.32		
$^{250}_{98}$Cf	0.283	2	2.65	6.49	2.59	13.42
		3	3.24	3.61		
		1	1.78	3.33		
$^{252}_{98}$Cf	0.288	2	2.69	6.96	2.64	14.11
		3	3.29	3.82		
		1	1.81	3.48		
$^{250}_{100}$Fm	0.280	2	2.59	5.91	2.54	12.87
		3	3.18	3.48		
		1	1.78	3.38		

E.B. Balbutsev, I.V. Molodtsova, "Scissors mode in transuranium elements", Eur. Phys. J. A60 (2024)185

I.V. Molodtsova, E.B. Balbutsev, , "Spin scissors mode in actinides", Int. J. Mod. Phys. E (2024)2441016

The scissors mode (SM) was investigated in the actinide region, including even–even superheavy nuclei up to ^{256}No. The trigger for this study was the recent reported observation by the Oslo group of the SM in the ^{254}No. The SM was studied within the Time Dependent Hartree-Fock-Bogoliubov (TDHFB) approach. The TDHFB equations were solved by applying the Wigner Function Moments (WFM) method.

The energy centroids and integrated M1 strengths for the transuranium nuclides up to ^{256}No are predicted. In all nuclei, scissors excitations are located in the energy from 1.7 to 3.3 MeV with centroids $\bar{E} = 2.5 - 2.6$ MeV. The total M1 strengths amount $\sum B(M1) = 11.5 - 13.5\,\mu_N^2$.

Calculations allow us to conclude that the observed double-humped structure of the scissors spectrum observed in the lightest actinides occurs due to the energy separation of excitations of conventional scissors and spin scissors.

The calculated summed strength in ^{254}No amounts $\sum B(M1) = 13.08\,\mu_N^2$, the centroid being located at the energy $\bar{E} = 2.52$ MeV. This results are in a good agreement with both the energy centroid and integrated M1 strength detected in experiment. Moreover, the calculated strength distribution is very similar to the observed one.

Table 3. The energies of lower (E_L) and upper (E_U) SMs and corresponding $M1$ strengths B_L and B_U. Experimental data (Oslo) are taken from Ref. 28.

	Lower SM				Upper SM			
	E_L (MeV)		$B_L(\mu_N^2)$		E_U (MeV)		B_U (μ_N^2)	
Nuclei	WFM	Oslo	WFM	Oslo	WFM	Oslo	WFM	Oslo
^{232}Th	2.17	1.95 ± 0.15	6.50	6.5 ± 2.2	3.06	2.85 ± 0.10	2.27	3.0 ± 1.2
^{238}U	2.32	1.95 ± 0.15	8.58	6.5 ± 1.2	3.22	2.90 ± 0.15	3.09	2.9 ± 1.0

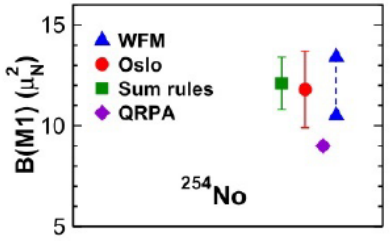

Fig. 2 The summed $M1$ scissors mode strength in ^{254}No obtained from WFM calculations (blue triangles) with the values $\beta_2 = 0.27$ (lower

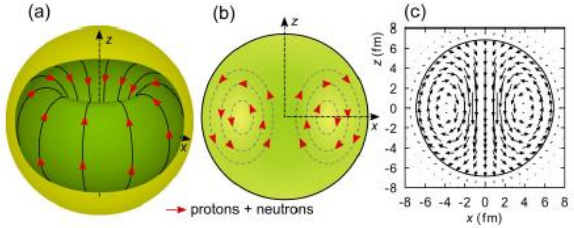

FIG. 1. Nuclear toroidal excitations. (a) Schematic view and (b) its cut in the x-z plane. (c) Same as (b) for the toroidal mode predicted in the nucleus ^{208}Pb [14]. The arrows mark the current along stream lines and their length is a measure of the current density.

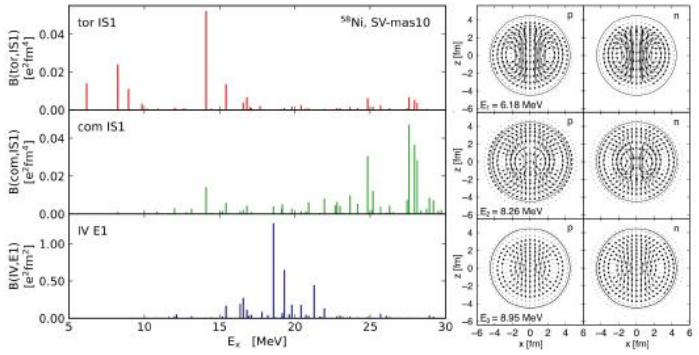

FIG. 2. Left: IS1 toroidal (top), IS1 compression (middle), and IV E1 (bottom) strengths in ^{58}Ni calculated with the DFT approach described in the text and the SV-mas10 interaction. Right: proton and neutron nuclear currents for the three lowest toroidal transitions.

V.O. Nesterenko, P.I. Vishnevskiy et al, "Candidate toroidal electric dipole mode in the spherical nucleus ^{58}Ni", Phys. Rev. Lett. 133(2024)232502

This work aims to identify candidates for low-energy E1 toroidal states (Toroidal Dipole Resonance) in ^{58}Ni. In the nuclear TDR nucleons exhibit small oscillations along the stream lines on the toroidal surface. Despite theoretical predictions ranging back more than 50 years, no experimental evidence of the nuclear TDR has been reported so far. The toroidal transition operator appears as second order term in the electric multipole operator

$$\hat{M}(E\lambda\mu, q) \approx \hat{M}(E\lambda\mu) + q\hat{M}_{tor}(E\lambda\mu).$$

Since dominant E1 transitions are mainly of isovector nature, their impact can suppressed by investigating isoscalar transition. Moreover, toroidal modes dominate over irrotational modes at backward angles in electron inelastic scattering.

Using a combination of experimental data from (e,e'), (p,p') and (γ, γ') reactions, the existence of low-energy E1 toroidal states in ^{58}Ni was predicted. The (e,e') data were thoroughly analyzed with the self-consistent random phase approximation (RPA) with Skyrme forces. It is demonstrated that transverse electron scattering form factors represent a relevant experimental observable to prove the toroidal nature of the states.

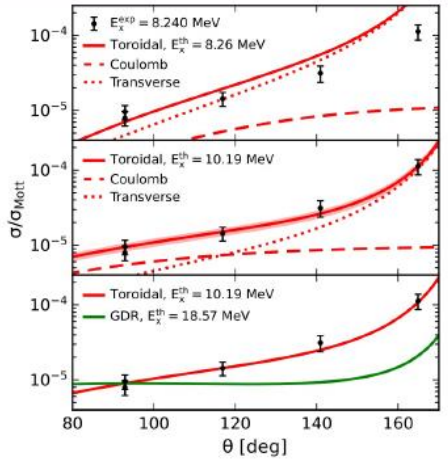

FIG. 3. Electron scattering cross sections of the toroidal candidate at 8.240 MeV [20] compared to QRPA predictions using the SV-mas10 interaction. Top: prominent theoretical toroidal excitation at 8.26 MeV. Middle: best fit result obtained as described in the text. Bottom: strongest theoretical isovector E1 transition (green line). The theoretical curves are normalized to the data at the most forward angle.

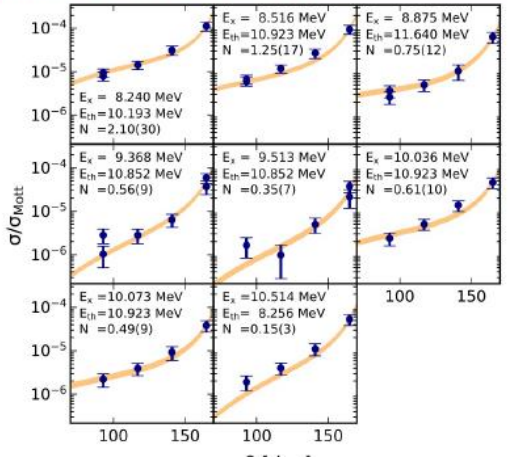

FIG. 4. Electron scattering cross sections (blue circles) of all toroidal candidates [20] compared with the best results from χ^2 fits of all theoretical $E1$ excitations below 11 MeV (orange bands). The energies of the QRPA states and the normalization factors N are quoted in the figure.

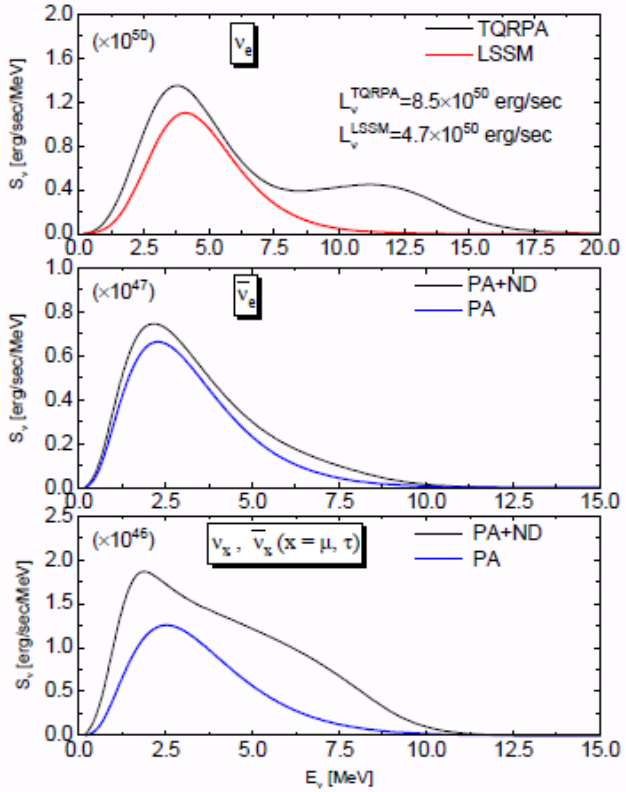

Figure 1: Total (anti)neutrino spectra obtained from the TQRPA and LSSM calculations.

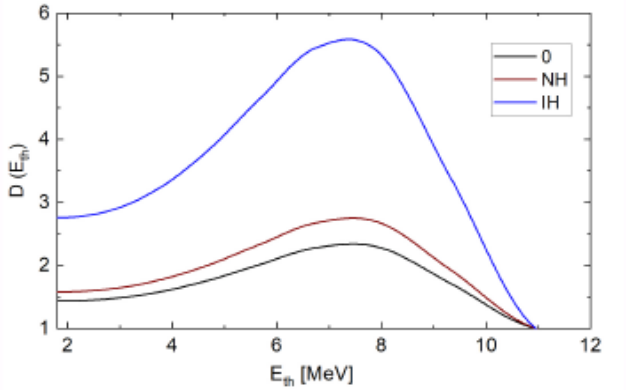

Figure 2: The $\bar{\nu}_e$ detection rate enhancement factor $D(E_{th})$ due to the ND procces as a function of the detector threshold energy E_{th} for the unoscillated spectrum (0), as well as for the normal (NH) and inverted (IH) hierarhies.

A.A. Dzhioev, A.I. Vdovin, A.V. Yudin, N.V. Dunina-Barkovskaya

1. Particles 6 (2023) 682

2. Monthly Notices of the Royal Astronomical Society 527 (2024) 7701

We propose a new method for calculating spectra and luminosities for (anti)neutrinos produced in the pre-supernova environment by weak processes with hot nuclei. It is based on the thermal quasiparticle random phase approximation (TQRPA), that allows microscopic thermodynamically consistent calculations of the weak-interaction response of nuclei at finite temperatures. For realistic representative pre-supernova conditions from the stellar evolution code MESA, we compute (anti)neutrino luminosities and spectra arising from neutral- and charged-current weak reactions with hot ^{56}Fe and compare them with the contribution of thermal processes.

We find that the TQRPA approach produces not only a higher total luminosity of electron neutrinos (mainly born in the electron capture reaction), compared to the standard technique based on the large-scale shell model (LSSM) weak-interaction rates, but also a harder neutrino spectrum. Besides, applying the TQRPA and LSSM, we find that in the context of electron antineutrino generation, the neutral-current nuclear de-excitation (ND) process via neutrino-antineutrino pair emission is at least as important as the electron-positron pair annihilation process. We also show that flavor oscillations enhance the high-energy contribution of the ND process to the electron antineutrino flux. This could potentially be important for pre-supernova antineutrino registration by the Earth's detectors.

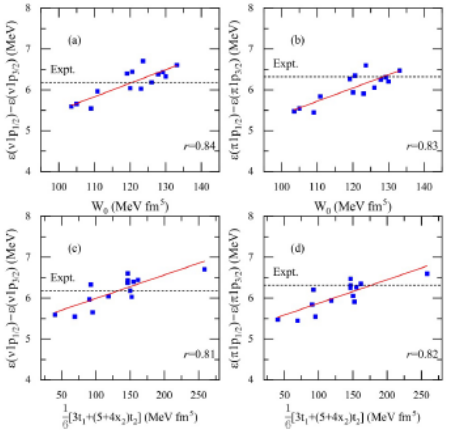

FIG. 1. Spin-orbit splitting for the neutron [(a) and (c)] and proton [(b) and (d)] $1p$ states in ^{16}O versus the value of spin-orbital potential W_0 [(a) and (b)] or versus the value of $\frac{1}{6}[3t_1 + (5 + 4x_2)t_2]$ [(c) and (d)] calculated using the 14 Skyrme EDFs. The correlation coefficients are shown. The experimental values of the spin-orbit splitting for $1p$ states are 6.18 and 6.32 MeV for neutron and proton [42], respectively.

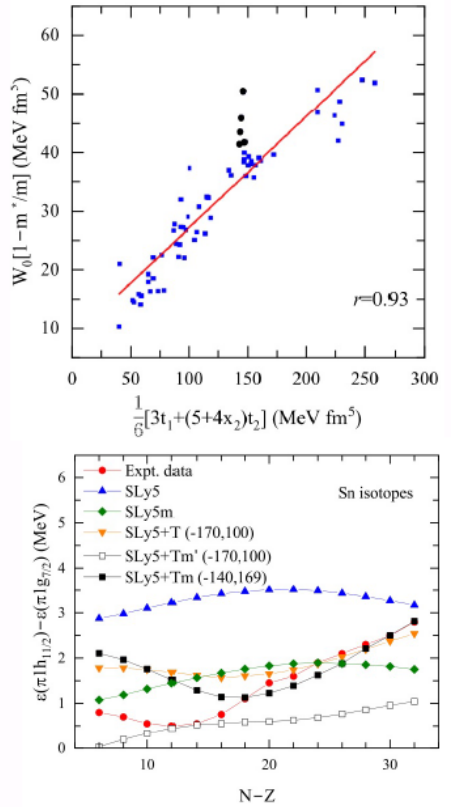

FIG. 3. Energy differences between the proton $1h_{11/2}$ and $1g_{7/2}$ levels along the tin isotopes. The experimental data are taken from Ref. [47]. See the text for details.

N.N. Arsenyev, A.P. Severyukhin, G.G. Adamian, N.V. Antonenko, "Correlation of spin-orbit potential and effective mass", Phys. Rev. C 110 (2024) 034312

In the RMF, the spin-orbit potential is connected to the effective mass as

$$V_{ls}^{q}(r) = \left(\frac{1}{r} \frac{\partial}{\partial r} \frac{1}{m_q^*(r)} \right) l \cdot s.$$

If we assume that in the Skyrme EDF the effective mass has the same origin as in the RMF, we obtain the relationship

$$W_0 = \frac{1}{6}[3t_1 + (5 + 4x_2)t_2].$$

This correlation can be used to reduce the number of parameters in Skyrme functionals.

The role of the spin-orbit interaction was considered together with the tensor force since these interactions affect the same observed quantities. As shown, the tensor force considerably improves the description of the isotopic dependence of the spin-orbit splitting. The use of the relation between W_0 and m^* in the Skyrme EDF does not spoil the description of experimental data. It even leads to a better description of the nuclear binding energies.

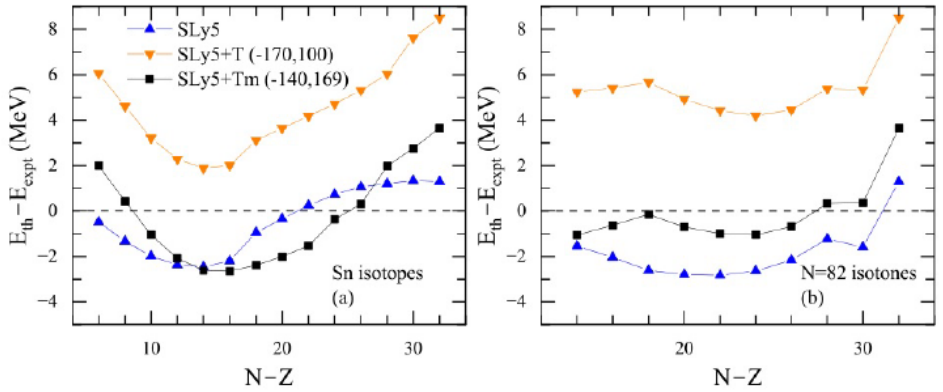

FIG. 8. Binding energy difference $E_{\rm th} - E_{\rm expt}$ along (a) $Z = 50$ isotopic and (b) $N = 82$ isotonic chains for the parametrizations indicated. Positive values of $E_{\rm th} - E_{\rm expt}$ denote overbound nuclei and negative values denote underbound nuclei. The experimental data are taken from Ref. [48].

A.Bahini,..., N.N. Arsenyev, A.P. Severyukhin,... NPA1059 (2025) 123078

Damping mechanism of the isoscalar giant monopole resonance in ^{58}Ni

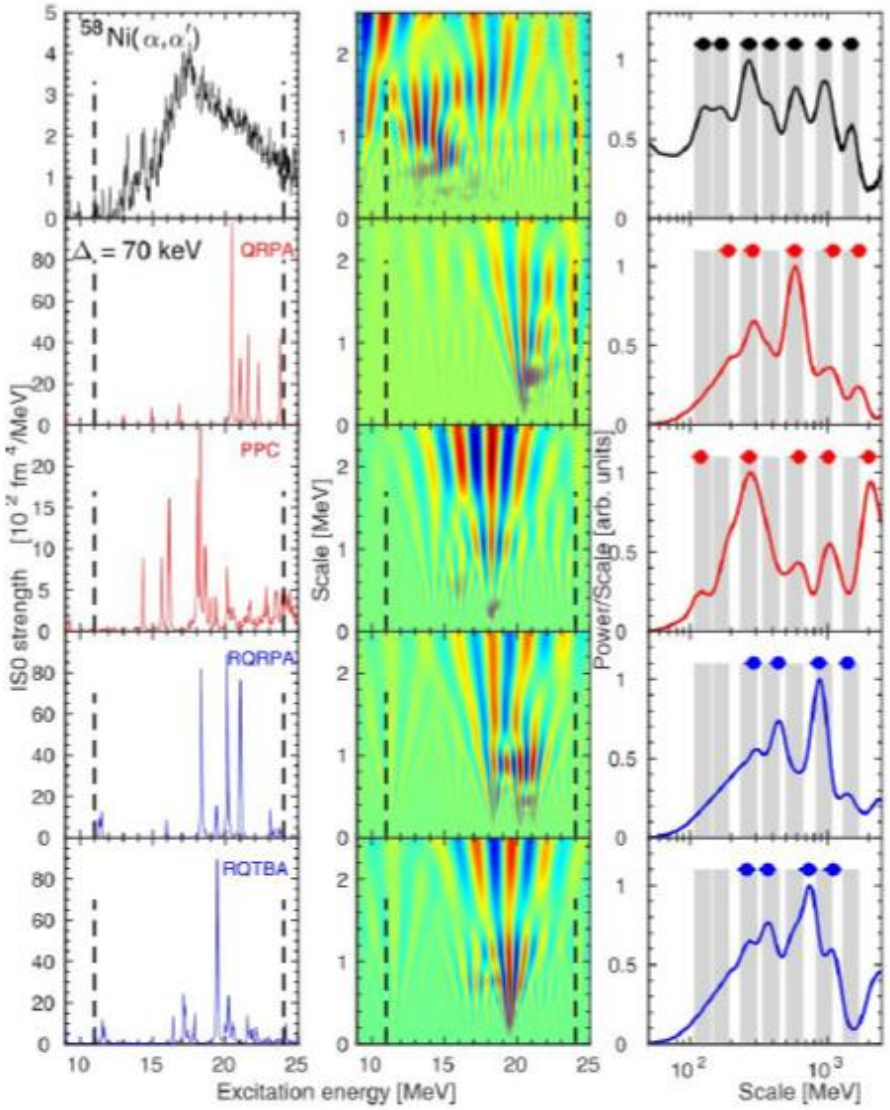

In this work, the fine structure of the isoscalar giant monopole resonance (ISGMR) and the contributions of various mechanisms to the formation of its decay width were investigated. To this end, the continuous wavelet transform method was employed to analyze the ISGMR strength distribution in ^{58}Ni, obtained experimentally at the iThemba Laboratory via alpha-particle scattering, as well as theoretical calculations incorporating coupling between simple and complex configurations. Wavelet analysis revealed characteristic energy scales inherent to the ISGMR strength distribution.

A comparison of the results demonstrated good agreement between experimental data and theoretical predictions. Consequently, it was shown that the dominant decay mechanism responsible for the ISGMR width is the coupling of simple particle-hole excitations with more complex two-particle–two-hole states.

R. V. Jolos, E. A. Kolganova

"Investigation of properties of 1^-_1 excited states of even-even nuclei"

Phys. Rev. C110 (2024) 014302

Characteristics of the lowest 1^- states that are of interest for study using the Compton source of monochromatic γ-rays are considered.

In near magic and close to them nuclei, the lowest 1^-_1 states have a quadrupole-octupole two-phonon structure. The collective nature of 1^-_1 states is followed from:

1. experimental data on excitation energies and E1 transition probabilities show a smooth dependence on mass number, which is typical for collective states
2. excitation energies of the 1^-_1 states which correlate with the sum of excitation energies of the 3^-_1 and 2^+_1 collective states
3. E1 $0^+_1 \to 1^-_1$ transitions that are characterized by relatively strong transition probabilities, which are 10^3 times stronger than typical low-energy E1 transitions.

A dramatic change in the spectrum of excited states of negative parity occurs in transition from spherical to deformed nuclei. The model was developed to describe the change in the structure and properties of low-lying negative parity excited states in this evolution from a spherical to a deformed shape.

The relationship between the experimental data characterizing the 1^-_1, 3^-_1 and 2^+_1 states was obtained.

Relations between different E1 transition matrix elements are derived and the parity dependence of E2 transitions is investigated.

Y. Chen, Q.B. Chen, R.V. Jolos

" Wobbling motion in octupole deformed nuclei "

Phys. Rev., C111 (2025) 064313

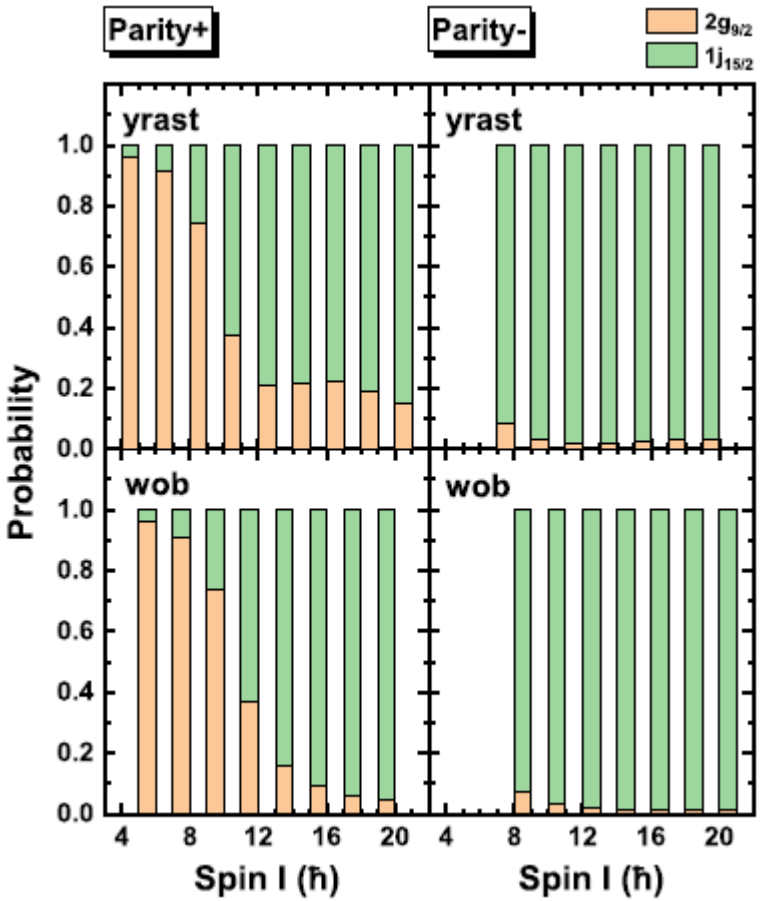

Probability distributions of spherical single-particle orbital angular momenta $P_{\alpha I}(j)$ for positive (left panels) and negative (right panels) parity bands.

The nuclear wobbling mode is uniquely related to triaxiality of nuclear shape. When the triaxial rotor is coupled to a high-j valence particle, there are two kinds of wobbling modes, namely, longitudinal (LW) and transverse (TW) wobbling.

Possible existence of wobbling motion in octupole deformed odd-A nucleus is explored for the $\pi(2g_{9/2}, 1j_{15/2})$ configuration based on octupole core-quasiparticle coupling model. Experimentally measurable physical quantities, such as energy spectrum, electromagnetic transition probability, g-factor, and SQM are studied. In addition, the probability distribution and angular momentum geometry are analyzed in detail.

Due to space reflection and axial symmetry breaking, positive and negative parity bands are formed, wobbling modes are established in each parity branch. Collective enhancement of intraband $B(E2)_{in}$ and the relative inhibition of interband $B(M1)_{out}$ confirm collective characteristics of wobbling motion.

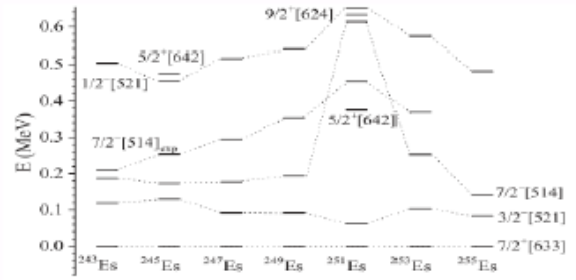

FIG. 2. Calculated spectra in isotopes of Es. Available experimental energies [56] of the $7/2^-$ state are indicated.

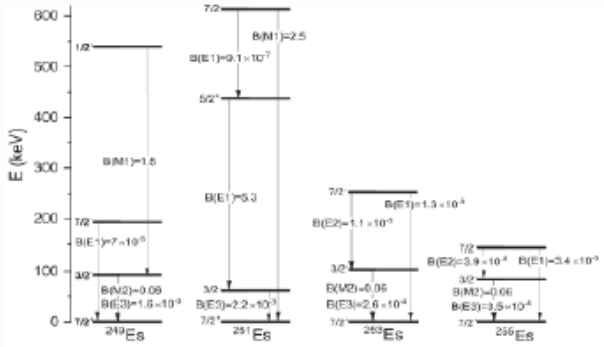

FIG. 4. The same as in Fig. 1, but for ^{249,251,253,255}Es.

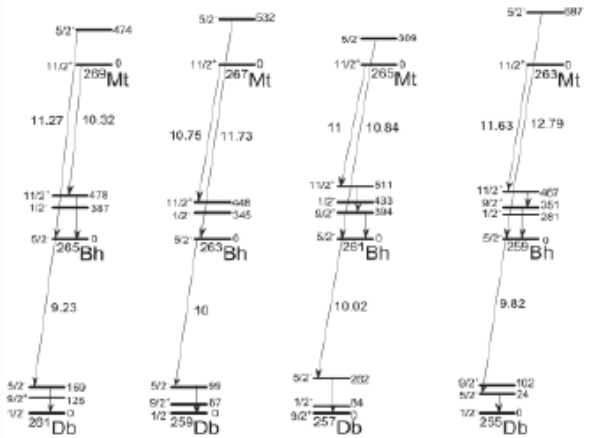

FIG. 11. Possible α-decay chains starting from ^{263,265,267,269}Mt. The calculated values of Q_α are given in MeV and the γ transitions following α decay are marked.

L.A. Malov, A.N. Bezbakh, G.G. Adamian, N.V. Antonenko, and R.V. Jolos, "Excitation spectra and electromagnetic transitions between low-lying nonrotational states of odd-proton nuclei with $Z = 97 - 109$", Phys. Rev. C 108 (2023) 044302

The systematic calculations of the excitation spectra, structure of the wave functions, and the γ-transition probabilities of odd-proton SH nuclei with $Z = 97 - 109$ were performed. The QPM was used to take into account the monopole pairing and the quasiparticle-phonon interaction. It is shown that the structure of nuclear states in the considered nuclei is mainly exhausted by the one-quasiparticle components. However, in some isotopes the quasiparticle$\otimes$phonon admixtures can play an important role. The quasiparticle-phonon interaction influences the ordering of the levels at the excitation energies characterized by quite dense excitation spectra and destroys the smooth isotopic dependence of state energies.

The calculated γ-transition probabilities allow us to find the isomeric states in the spectra of nuclear excitations and estimate the lifetimes of isomers.

The α-decay chains starting from ^{263,265,267,269}Mt were analyzed. The nuclei in these α-decay chains have either one or two α-decay lines. The number of α-decay lines can depend on whether the nucleus is produced directly or after the α- decay of the parent nucleus. This fact deserves experimental study.

The calculated excitation spectra of the considered nuclei being compared with the experimental ones will give us information on the mean field potentials of heavy nuclei. This information is of great importance for calculations of the survival probabilities of superheavy nuclei.

V.O. Nesterenko, M.A. Mardyban et al, PRC111 (2025)064322

Low-energy spectra of nobelium isotopes: Skyrme random-phase approximation analysis

TABLE XIII. The energies (in MeV) of the lowest neutron and proton 2qp 8^- states in ^{252,254}No, calculated with UNEDF1, UNEDF1^{SO}, and UNEDF2.

	UNEDF1	UNEDF1^{SO}	UNEDF2
^{252}No, $E_x = 1.254$ MeV			
$nn[624\downarrow, 734\uparrow]$	0.870	0.954	1.119
$pp[624\uparrow, 514\downarrow]$	1.242	1.279	1.430
^{254}No, $E_x = 1.295$ MeV			
$nn[624\downarrow, 734\uparrow]$	1.036	1.141	1.338
$nn[613\uparrow, 734\uparrow]$	1.081	1.321	1.605
$pp[624\uparrow, 514\downarrow]$	1.190	1.250	1.390

TABLE XIV. Experimental and calculated energies (in MeV) of $K^\pi = 2^-$ isomer $nn[622\uparrow, 734\uparrow]$ in ^{252}No and 3^+ isomer $pp[521\downarrow, 514\downarrow]$ in ^{254}No.

	Exp.	UNEDF1	UNEDF1^{SO}	UNEDF2
2^- in ^{252}No	0.929	0.991	1.141	1.207
3^+ in ^{254}No	0.987	0.695	1.168	0.880

Low-energy spectra in the isotopic chain $^{250\text{-}262}$No are systematically investigated within the fully self-consistent QRPA using Skyrme forces SLy4, SLy6, SkM*, and SVbas. In ^{252,254}No, a reasonable description of $K^\pi = 8^-, 2^-, 3^+$ isomers is obtained with SLy4 and SLy6. For the 8^- isomer in ^{254}No, a neutron nature (configuration $nn[734\uparrow, 613\uparrow]$) was confirmed.

For a more accurate treatment of pairing correlations within the LN approximation, the forces UNEDF1, UNEDF1S0, and UNEDF2 were applied. However, despite a more realistic treatment of the pairing, the UNEDF forces do not provide a simultaneous reasonable description of 8^-, 2^- isomers in ^{252}No and of 3^+, 4^+ isomers in ^{254}No.

The comparison of SLy4 and SLy6 results shows that, in the case of shell gaps, even tiny changes in the single-particle spectra can noticeably affect the pairing and related nuclear properties.

TABLE IV. Characteristics of the lowest ($\nu = 1$) calculated 8^- states in ^{252,254}No: QRPA excitation energies E_ν, reduced transition probabilities $B(E98)$, main 2qp components qq', their energies $\epsilon_{qq'}$, contributions to the state norm $N_{qq'}$, and F order. For convenience of discussion, for ^{254}No the second ($\nu = 2$) 8^- states are also depicted.

Force	E (MeV)	$B(E98)$ (W.u.)	qq'	$\epsilon_{qq'}$ (MeV)	$N_{qq'}$	F order
^{252}No, $E_x = 1.254$ MeV						
SLy4	1.257	0.022	$nn[624\downarrow, 734\uparrow]$	1.211	0.998	F,F+1
SLy6	1.361	0.038	$nn[624\downarrow, 734\uparrow]$	1.317	0.996	F,F+1
SkM*	1.330	0.025	$nn[734\uparrow, 624\downarrow]$	1.198	0.992	F,F+1
SVbas	1.913	0.119	$nn[624\downarrow, 734\uparrow]$	1.751	0.912	F,F+1

A.A. Dzhioev, N.V. Antonenko, PRC112 (2025) 03433

Isoenergetic description of induced fission pathways within energy-density functional theory

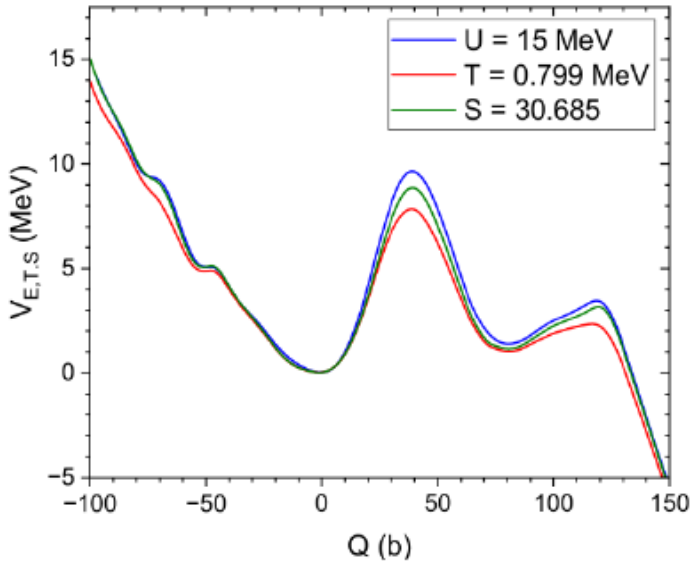

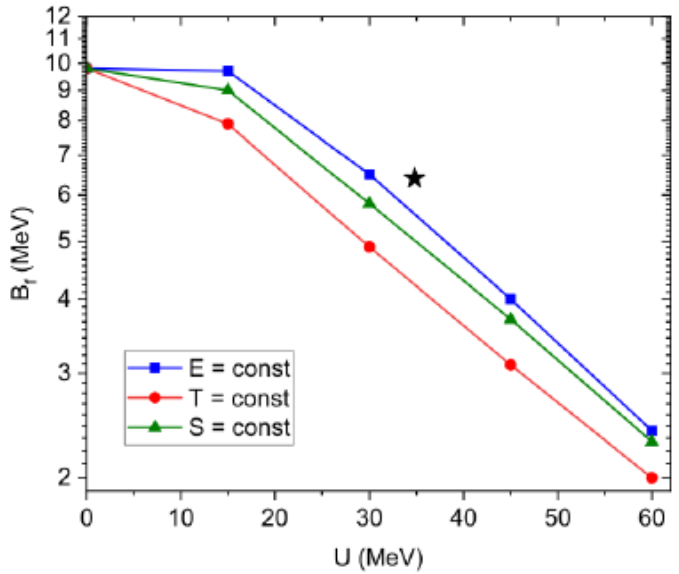

An isoenergetioc description of fission pathways in excited nuclei is developed within the framework of nuclear energy-density functional theory. Using self-consistent finite-temperature Hartree-Fock-Bogoliubov calculations with the Skyrme-type energy-density functional SkM*, we derive and compare effective potentials for ^{296}Lv corresponding to different thermodynamic processes - isothermal (T=const), isentropic (S=const), and isoenergetic (E=const) - as functions of quadrupole deformation and excitation energy. It is shown that at the same amount of excitation energy the isoenergetic description predicts the highest fission barrier and the largest damping factor. The suppression of the isoenergetic fission barrier is analyzed by examining how the driving force changes with increasing excitation energy and by studying the contribution of the nonpotential term to the effective potential. Within the framework of the three thermodynamic schemes considered, the different behavior of temperature and entropy along the fission pathway is also emphasized.

Physics Letters B 844 (2023) 138099

Contents lists available at ScienceDirect

Physics Letters B

journal homepage: www.elsevier.com/locate/physletb

Multi-step particle emission probabilities in superheavy nuclei at moderate excitation energies

A. Rahmatinejad [a], T.M. Shneidman [a,1], G.G. Adamian [a,*], N.V. Antonenko [a,b], P. Jachimowicz [c], M. Kowal [d]

[a] Joint Institute for Nuclear Research, Dubna, 141980, Russia
[b] Tomsk Polytechnic University, 634050 Tomsk, Russia
[c] Institute of Physics, University of Zielona Góra, Szafrana 4a, 65516 Zielona Góra, Poland
[d] National Centre for Nuclear Research, Pasteura 7, 02-093 Warsaw, Poland

ARTICLE INFO

Article history:
Received 5 July 2023
Received in revised form 21 July 2023
Accepted 24 July 2023
Available online 28 July 2023
Editor: B. Balantekin

Keywords:
Superheavy nuclei
Microscopic-macroscopic model
Fission

ABSTRACT

The probabilities of *xn*-, *pxn*-, and αxn-evaporation channels in excited superheavy nuclei were evaluated using the Monte Carlo method. The calculations utilized microscopically determined nuclear level densities and were compared with results obtained from the phenomenological Jackson formula. Effective temperatures derived from the microscopic approach were incorporated into the Jackson formula for different evaporation channels at low and moderate excitation energies. Additionally, an analytical formula was introduced to estimate the average kinetic energy of emitted particles in multi-step processes.

© 2023 The Author(s). Published by Elsevier B.V. This is an open access article under the CC BY license (http://creativecommons.org/licenses/by/4.0/). Funded by SCOAP[3].

I. S. Rogov, G. G. Adamian, N. V. Antonenko

"Is there an abrupt fall of spontaneous fission half-lives in ^{248}No and ^{252}Rf?"

Eur. Phys.J. A60 (2024) 164

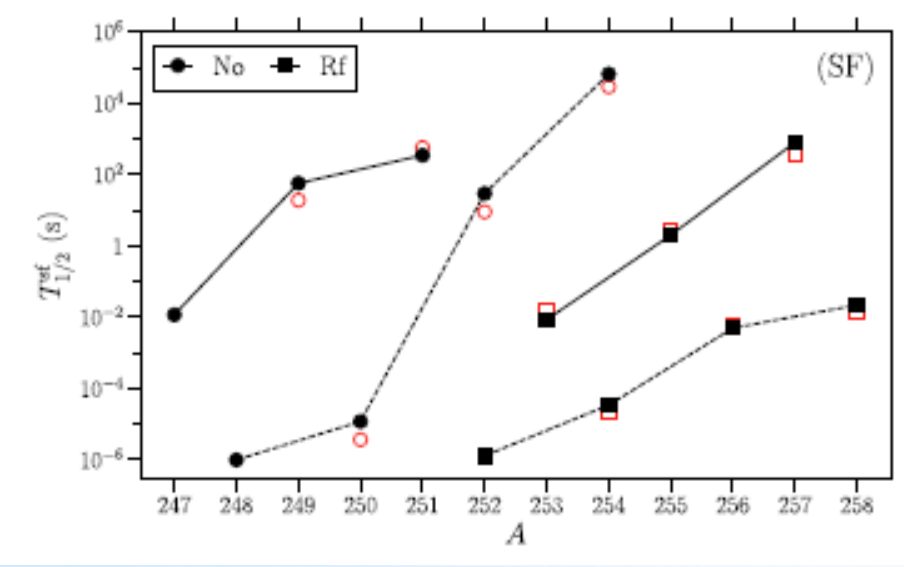

Experimental (open red symbols) and calculated SF half-lives for $^{247-252,254}No$ (circles) and $^{252-257}Rf$ (squares)

Spontaneous fission (SF) terminates nuclear stability in the region of heavy nuclei. The study of the relation of partial half-lives of the competing decay modes for the isotopes of the transfermium region is essential to understanding their production rates in nuclear synthesis.

A strong reduction (about 5, 6 orders of magnitude) in the SF half-lives $T_{1/2}$ between No and Rf isotones (N = 152, 150,149) was found. Assuming the same trend for the N = 148 and 149 isotones, one can expect a large decrease in the half-life of ^{252}Rf in comparison to ^{250}No. The aim is to predict the lifetimes of nuclei ^{248}No and ^{252}Rf in the ground state.

Spontaneous fission and α- decay from the ground state of nuclei ^{248}No and ^{252}Rf are studied within dinuclear system model. All these decay processes are considered as the evolution of a nucleus in the charge (mass) asymmetry coordinate. For the even-even and even-odd nobelium and rutherfordium isotopes, the available experimental spontaneous fission and α-decay half-lives of the ground state are well described.

No abrupt decreases in $T_{1/2}$ of the neutron-deficient No and Rf isotopes are predicted within the cluster model.

N.S. Moiseev, N.V. Antonenko, G.G. Adamian

" Empirical systematics of spontaneous fission half-lives of heavy and superheavy nuclei "

Phys. Rev. C112 (2025) 034607

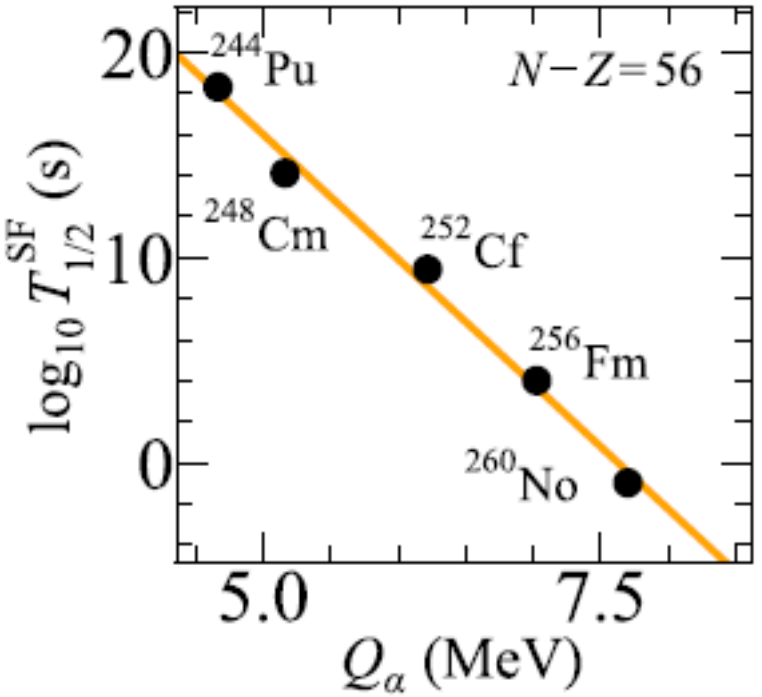

Logarithm of the experimental SF half-lives as a function of experimental energy release Q_α for nuclei with $94 < Z < 102$ and fixed values of the neutron excess (N - Z) (black circles) and their fit (orange lines).

Spontaneous fission (SF) is observed in nuclei with $A > 230$ and exhibits a wide range of experimental half-lives $T^{SF}_{1/2}$, spanning from 10^{-5} to 10^{29} s.

A linear correlation is found between Logarithm of the spontaneous fission half-lives $T^{SF}_{1/2}$ and energy release Q_α of alpha decay for nuclei with the same neutron excess (N - Z) and atomic numbers in the range $90 \leq Z \leq 102$.

New semiempirical formula, which depends on experimental observables rather than calculated shell-correction energy or shape-dependent liquid-drop mass formula, was proposed for the half-lives of SF nuclei, depending on both Q_α and (N - Z).

Model implies a mutual connection between α-decay, cluster radioactivity and SF phenomena in nuclei that exhibit these decay modes.

A. Nasirov, E. Khusanov, B. Kayumov,
O. Ganiev, A. Yusupov, A. Safarov

" The effect of the entrance channel properties in formation of the reaction products in heavy ion collisions "

Nucl. Phys. A 1065 (2026) 123262

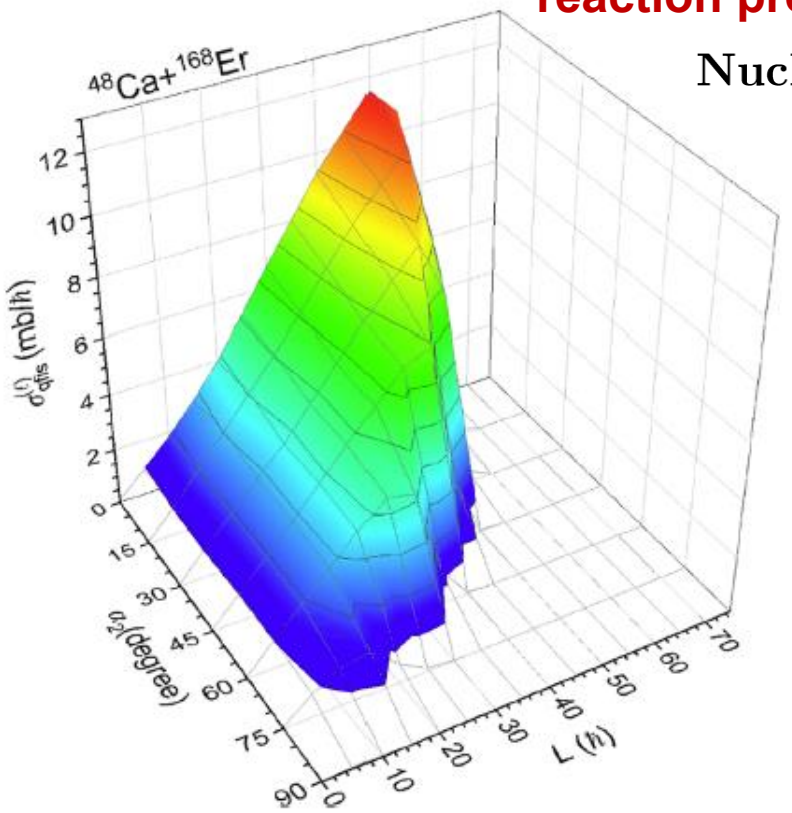

Partial quasifission cross section calculated for ^{48}Ca + ^{168}Er reaction at E_{Lab} = 194 MeV as a function of the orbital angular momentum L and orientation angle of the axial symmetry axis of target nucleus ^{168}Er.

Synthesis of superheavy elements shows: there is a huge hindrance for complete fusion in the reactions with massive nuclei.

Competition between complete fusion and quasifission on the mass asymmetry of the entrance channel, on initial orbital angular momentum and orientation angles of the colliding nuclei have been considered in the framework of the a dinuclear system model.

Hindrance is explained by the increase of intrinsic fusion barrier B_{fus}. Thus, yield of quasifission products strongly increases. Yields of quasifission calculated in ^{48}Ca + ^{168}Er and ^{12}C + ^{204}Pb leading to the CN $^{216}Ra^*$ with the same excitation energy around E^*_{CN} = 40 MeV in both reactions. Analysis showed that the contribution of quasifission products to the mass asymmetric region of the fusion-fission products in the case of ^{48}Ca + ^{168}Er reaction is much larger than the one observed in ^{12}C + ^{204}Pb reaction.

Sh.A. Kalandarov, G.G. Adamian, N.V. Antonenko, J. Busa, Jr.

" Roles of driving potential and thresholds of particle emission from a compound nucleus in the production of evaporation residues "

Phys. Rev. C111, (2025) 034620

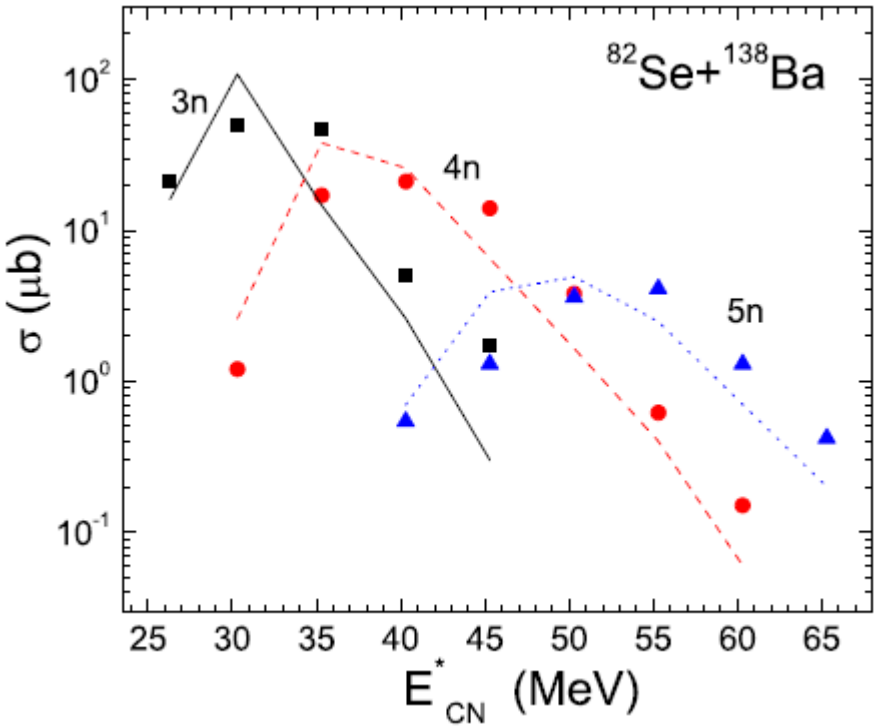

Comparison of calculated (lines) and experimental (symbols) excitation functions in the xn evaporation channels for reaction leading to CN $^{220}Th^*$.

The influence of driving potentials and thresholds of particle emission from a compound nucleus on the formation of evaporation residues is studied in complete fusion reactions within the dinuclear system model.

The formation of ER in the xn, pxn, and αxn evaporation channels was analyzed for complete fusion reactions leading to the same CN as $^{200}Po^*$, $^{216,222}Th^*$, and $^{224}U^*$.

Experimental maximum production cross sections and excitation functions of evaporation residues in the xn, pxn, and αxn channels of complete fusion reactions leading to compound nuclei with atomic numbers $Z_{CN} = 84$, 90, and 92 are well described and several predictions are made.

H. Pasca, A. V. Andreev, G. G. Adamian , and N. V. Antonenko

"Excitation-energy dependence of the fission-fragment neutron-excess ratio "

Phys. Rev. C107 (2023) 024603

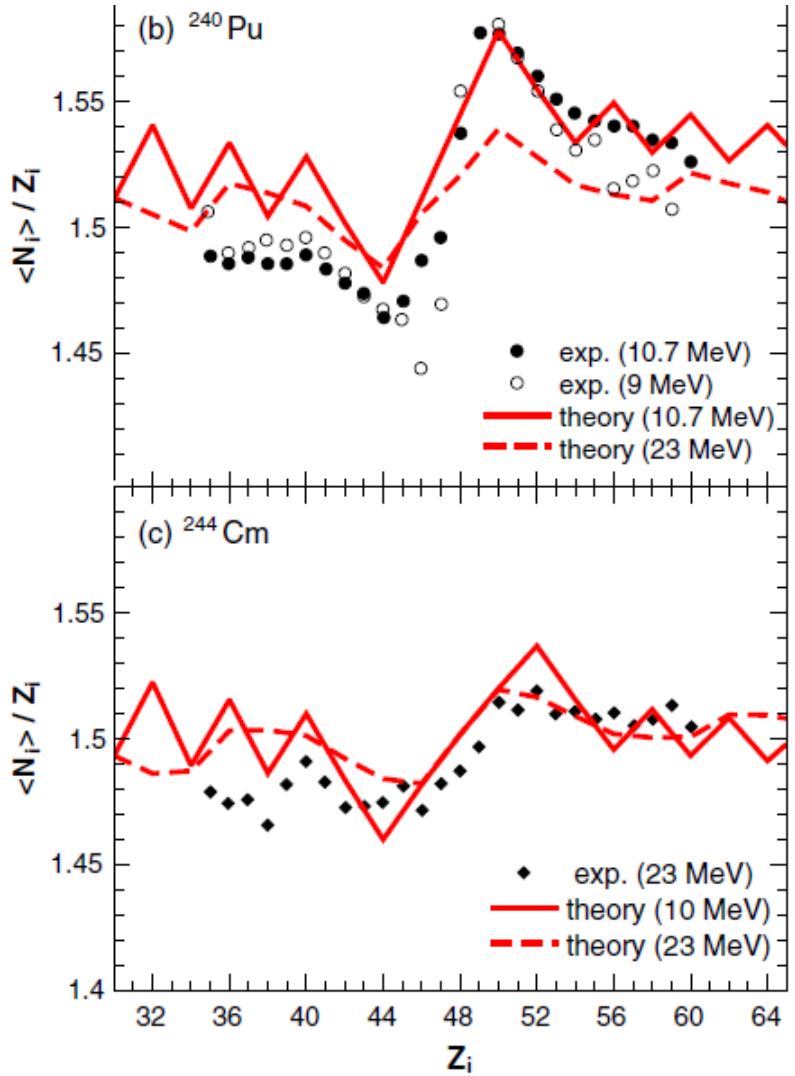

The fission observables are described within an improved scission-point model. Model assumes that the fission observables are mainly established at the scission configurations (dinuclear systems with two touching individual fragments).

For the induced fission of ^{238}U, ^{240}Pu, ^{244}Cm, and ^{250}Cf, the dependencies of the fission-fragment neutron-excess ratio on the shell structure and excitation energy of fragment are studied.

Conclusion: the low-energy fission shows that the neutron-excess ratio $\langle N_i \rangle / Z_i$ of fission fragments has a strong dependence on the fragment charge number Z_i, exhibiting a well-defined sawtooth structure, which is the direct result of the interplay between the neutron and proton shell closures.

T.M. Shneidman, A. Rahmatinejad, G.G. Adamian, N.V. Antonenko

" Quantum-mechanical description of angular motion of fission fragments at scission "

Phys. Rev. C 111 (2025) 064621

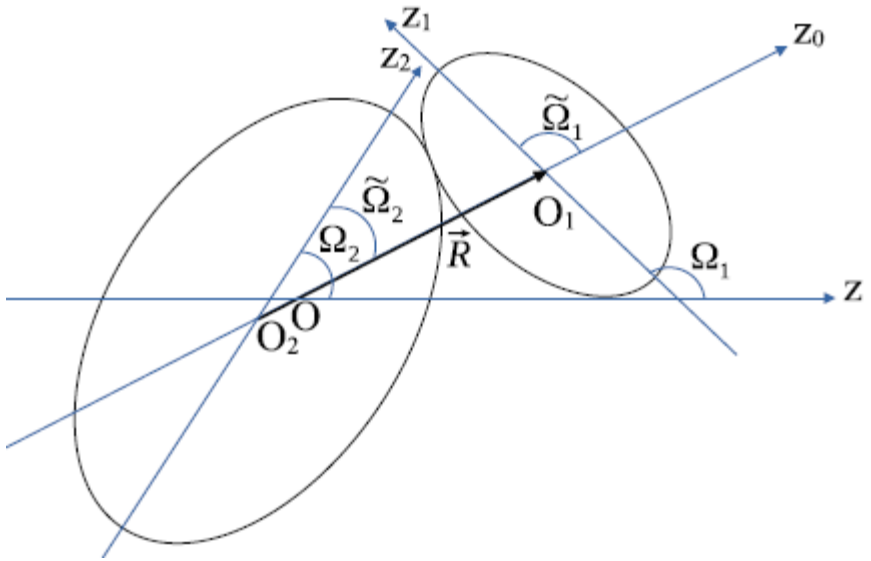

Schematic picture of angular motion in the DNS. Laboratory system is Oz. Body-fixed system Oz0: z axis coincides with vector of relative distance R. The orientations of body-fixed system and intrinsic systems of the fragments are defined by the Euler angles Ω_i.

A model for quantum mechanical treatment of angular motion in the system consisting of two fission fragments at touching configuration was proposed.

It was shown, unlike the bending/wriggling scenario, this motion can be considered as small-amplitude independent vibrations of fragments around pole-to-pole configuration. Angular momentum generated by vibrations is balanced by relative rotation of DNS fragments.

The model allows to explain the absence of correlation between the angular momenta generated in primary fission fragments. Distribution of projection of angular momenta of the fragments on the separation axis is peaked around either $K = 0$ or $K = 1$, but it extends well to $K \approx 4$. The model explains the saw-tooth pattern in the angular momentum as a function of fragment mass.

A.V.Isaev , … , A.V.Andreev , … , A.Rahmatinejad , … ,T.M.Shneidman, …

“ Structure of the prompt neutron multiplicity distribution in the spontaneous fission of ^{256}Rf ”

Phys. Lett. B 843 (2023) 138008

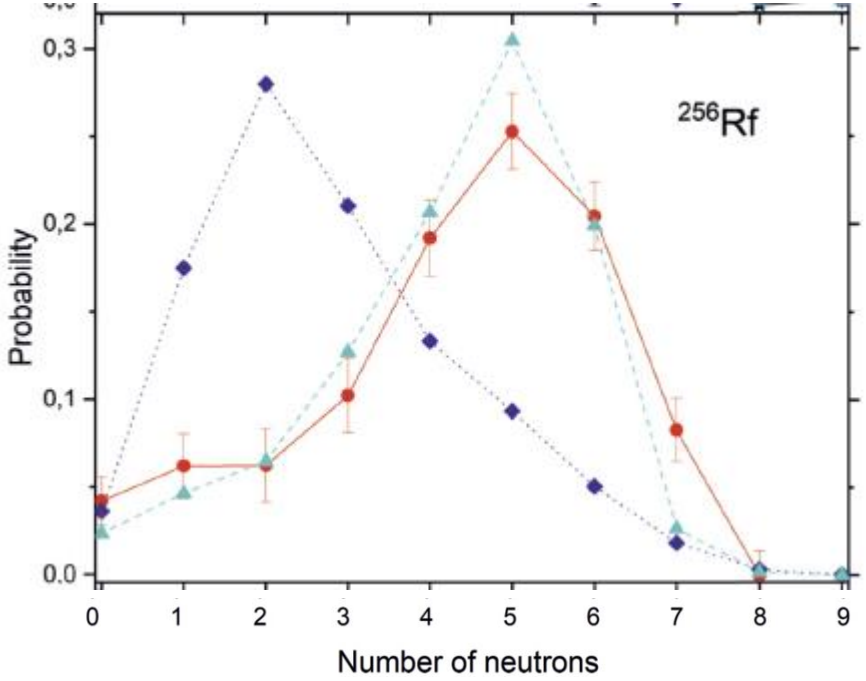

Prompt neutron emission probability distributions for ^{256}Rf. Experimental data: circles. ISP model – △ , GEF model – ◊.

For the first time, a detailed experimental study of the neutron multiplicity distribution in the spontaneous fission of superheavy nuclei ^{256}Rf is presented.

The theoretical calculations of neutron multiplicity were carried out in the frame of the improved scission point model (ISP).

The potential energy surface is calculated in the mic-mac approach with an account for the shell corrections of the fragments and their damping with excitation energy.

The experimental results for ^{256}Rf are compared with predictions made by the ISP model and the agreement found in the average number of neutrons is good and the shape of the model distribution is quite close to the experimental one.

H. Pasca, G.G. Adamian, N.V. Antonenko

" Alpha clusterization as a reason for the narrow symmetric mass distribution in spontaneous fission of ^{258}Fm "

Phys. Lett. B870 (2025) 139943

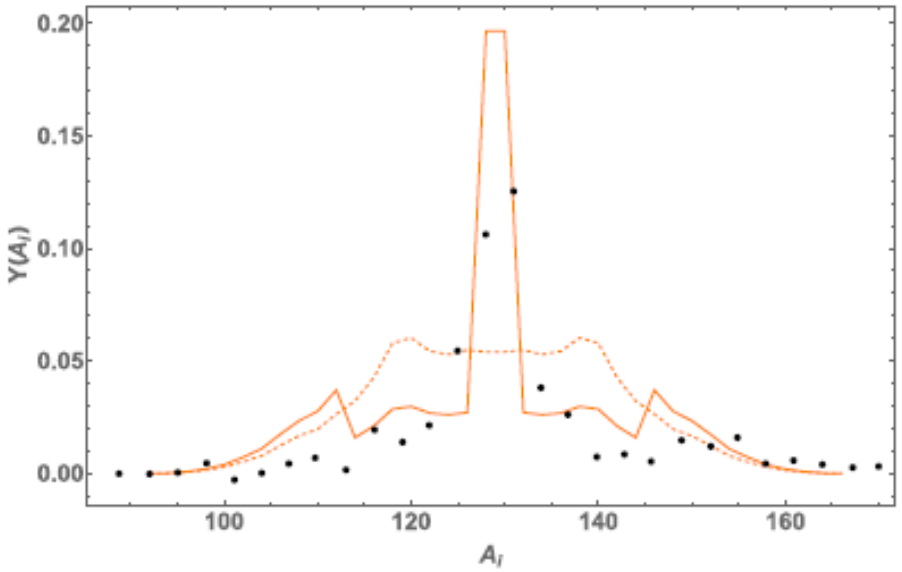

Mass yields of SF of ^{258}Fm resulting from usual binary decays and binary decays with contributions of trinuclear systems are shown by dashed and solid lines, respectively. Experimental data - symbols.

Spontaneous fission (SF) of ^{258}Fm results in the narrow symmetric mass distribution of fragments, while the total kinetic energy (TKE) distribution of fragments appear to be composed of two modes with peaks located near 204 and 232 MeV.

SF of ^{258}Fm was explained within the micro-macro models by existence of two fission modes. Another explanation was suggested. It is based on the α-particle clustering of heavy fragment in the mass-asymmetric scission configuration. The main goal is to simultaneously describe the mass distribution and TKE in SF of ^{258}Fm.

Unusually narrow symmetric mass distribution of ^{258}Fm(SF) can be related to α-clustering of heavy fragment in the DNS Cd+Te and formation of trinuclear systems Cd+α+Sn and their binary decays leading to formation of Sn fragments. Large variation of TKE distribution of fission fragments was also explained by existence of fission pathway through the binary scission of trinuclear systems.

Sh. A. Kalandarov , R.B. Tashkhodjaev , O.K. Ganiev

"Formation mechanism of decay fragments in spontaneous ternary fission of heavy nuclei "

Phys. Lett. B850 (2024) 138522

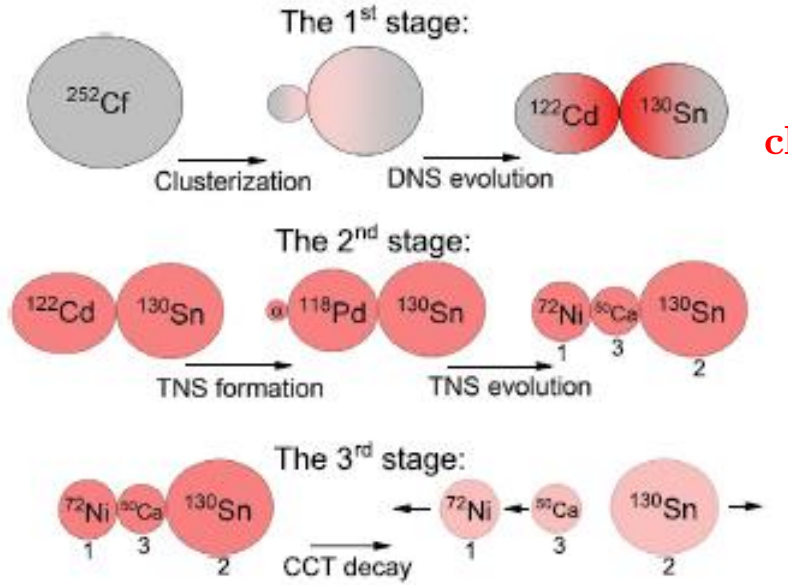

Mechanism of formation of collinear cluster tri-partition (CCT) fragments.

Experimental ratio for different types of ternary fission to binary one

symmetric (nearly equal masses) $\sim 2 \times 10^{-9}$

asymmetric (lightest fragment A > 30) $\sim 8 \times 10^{-8}$

charged particle (mainly α) accompanied fission $\sim 3 \times 10^{-3}$

collinear cluster tri-partition (CCT) $\sim 4 \times 10^{-3}$

The model is developed in which spontaneous ternary fission takes place in three consecutive stages:

1. the formation of asymmetric DNS and its evolution in mass (and charge) asymmetry coordinates towards symmetric DNS configurations
2. the transformation of one of the nearly symmetric DNS nuclei into another DNS, thus forming the TNS
3. the decay of TNS into three fragments.

The presented model of spontaneous ternary fission describes well the experimentally observed features and quantities of spontaneous ternary fission of ^{252}Cf.

G. G. Adamian, N. V. Antonenko, H. Lenske, V. V. Sargsyan

"Application of a universal reaction function to the description of heavy-ion reaction cross sections"

Phys. Rev. C109 (2024) 014602

Often the comparison of different reactions is more instructive to perform by using the dimensionless quantities to suppress trivial differences, arising mostly from sizes and charges of the collision partners. Follow this approach it is possible to derive the analytical expression (universal fusion function UFF) for fusion cross sections. However, the reduction procedure is not unique.

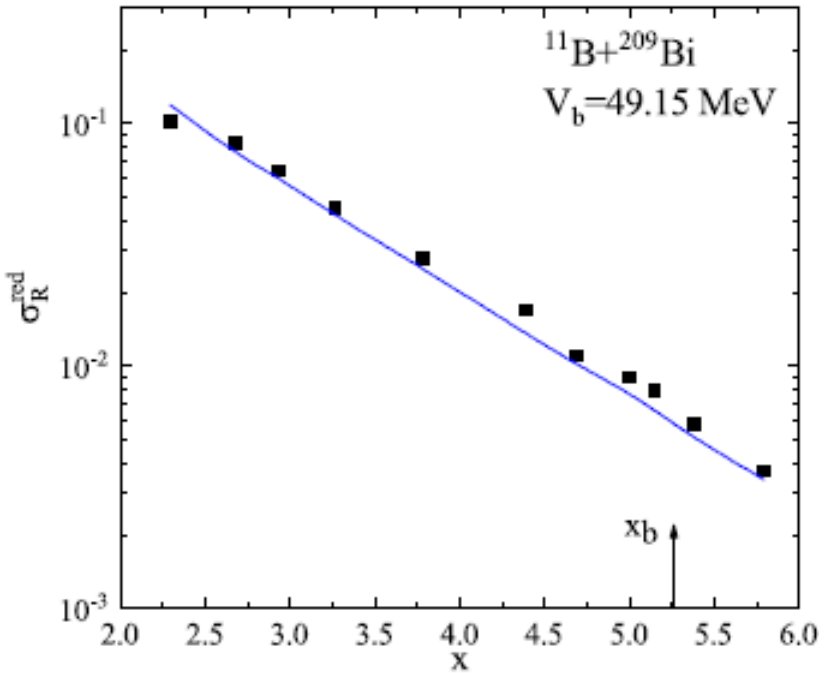

Comparison of the reduced experimental reaction cross sections (symbols) with the URF (lines) versus x.

By analogy to UFF the universal reaction function (URF) was suggested for the heavy-ion reaction cross section.

To get URF the two approximations have been used:

1. the analytical formula for the elastic scattering probability
2. the reaction probability at given angular momentum J was simulated by the reaction probability at $J = 0$ but evaluated at the energy shifted on the value of the rotational one.

The new formulas describe the experimental data well and can be used for the analysis and predictions of heavy-ion reaction cross sections.

$$x = (E - V_b)/(\hbar\omega_b)$$

V. V. Sargsyan, G. G. Adamian, N. V. Antonenko

"Astrophysical *S-factors for complete fusion reactions* $^{12,13}C + ^{12,13}C$"

Eur. Phys.J. A60 (2024) 180

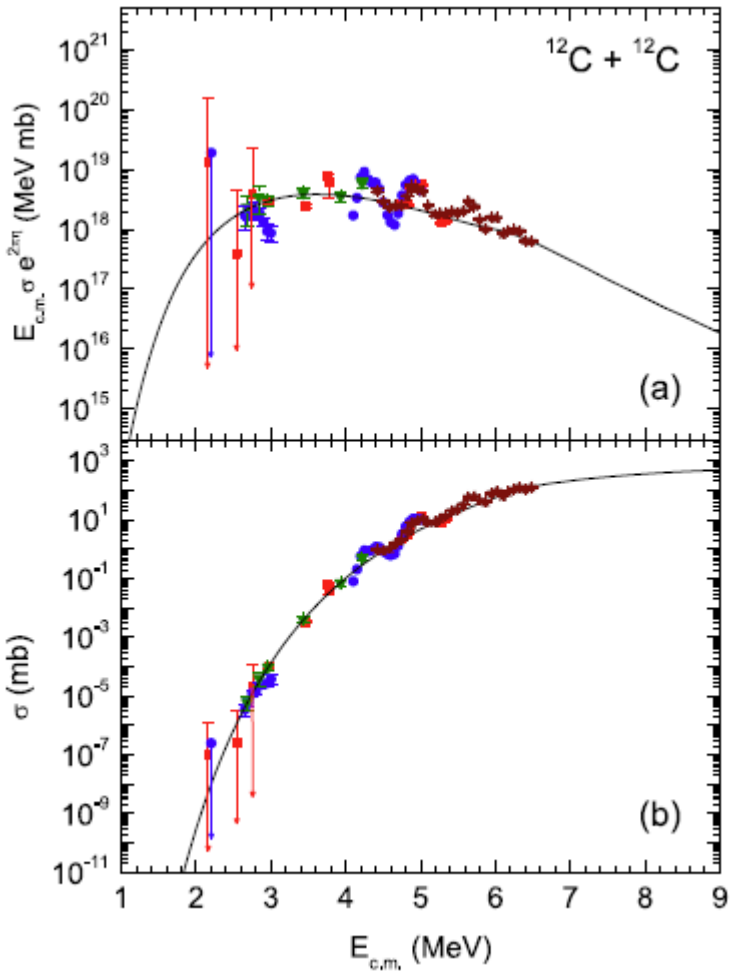

The calculated astrophysical S-factor (a) and fusion excitation function (b) for the $^{12}C + ^{12}C$ reaction.

The fusion reactions of various carbon isotopes are of exceptional importance for astrophysics. These reactions become key processes for the production of elements up to the iron region.

The energy range of interest (Gamow window) for carbon fusion is 1-3 MeV in the c.m. system. Experimental data are limited. Presence of a maximum in astrophysical S-factor remains debatable.

Comparative analysis of the complete fusion reactions $^{12}C + ^{12}C$, $^{12}C + ^{13}C$ and $^{13}C + ^{13}C$ at extremely low energies is performed using the Extended Quantum Diffusion Approach.

The theoretical calculations are compared with the available experimental data, and the results are discussed for future experiments. The study reveals the presence of a maximum in the astrophysical S-factor for these reactions.

W.M. Seif, V.V. Sargsyan, G.G. Adamian, N.V. Antonenko

" Role of internal kinetic energy in the surface density-overlap region of fusing nuclei "

Phys. Rev. C111 (2025) 044307

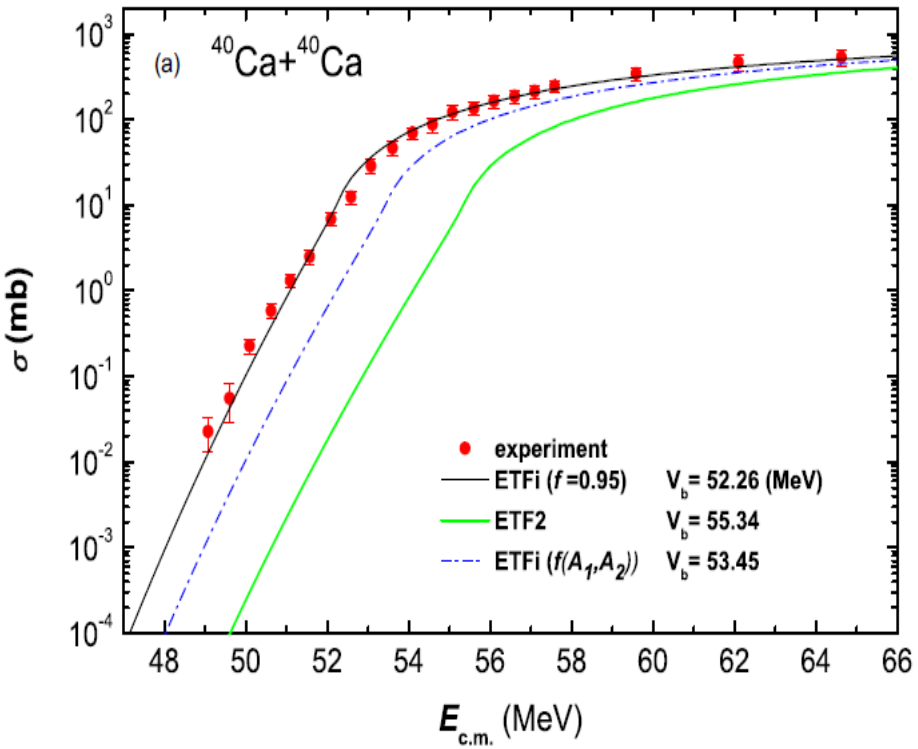

Complete fusion excitation functions for ^{40}Ca + ^{40}Ca reaction calculated using different ETFi approximation. symbols - experimental data.

Many energy-density functionals are based on extended Thomas-Fermi (ETF) approximation to express the internal kinetic-energy densities as functions of the corresponding nucleon densities and their derivatives.

Density overlap between two interacting nuclei results in a change of the internal kinetic energy, which magnifies a repulsive contribution.

Fusion reactions were used to examine repulsive internal kinetic energy contribution to the nucleus-nucleus interaction potential with several approximations of kinetic-energy density.

Usual ETF approximations fail to correctly describe the complete fusion process. Modification of the internal kinetic-energy density functions are suggested, with which the fusion cross sections are successfully reproduced.

S. A. Rakityansky , S. N. Ershov

“Calculating the width of an ultranarrow quantum resonance”

Phys. Rev. C109 (2024) 034609

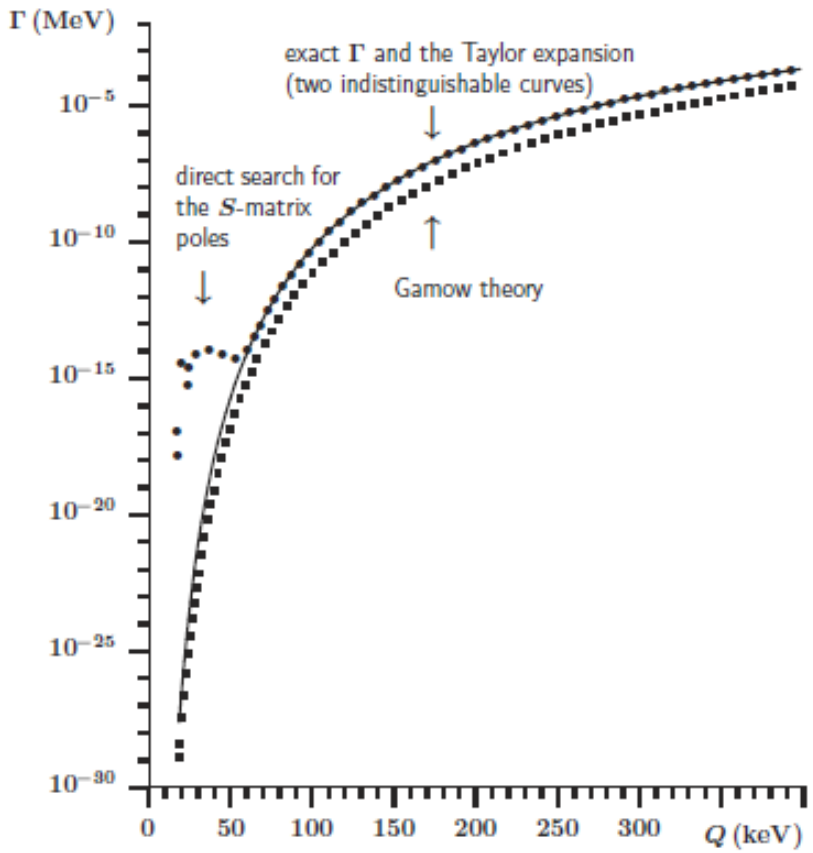

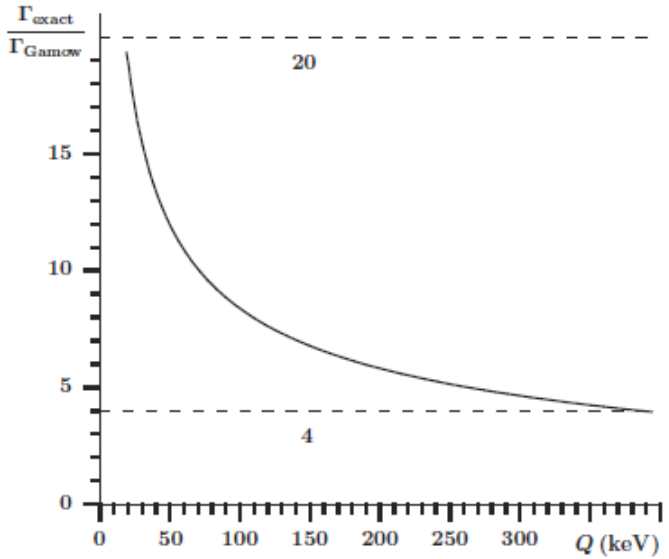

A reliable way of calculating the width Γ of an extremely narrow quantum resonance is suggested. The proposed method is based on expanding the Jost function in the Taylor series around the real resonance energy E_r and looking for its zero at the nearby complex point $E_r - i\Gamma/2$. The coefficients of such an expansion can be obtained by solving a set of coupled differential equations. Using two simple exactly solvable models, it is demonstrated that the method is efficient and accurate.

Eur. Phys. J. A (2025) 61:79
https://doi.org/10.1140/epja/s10050-025-01549-x

THE EUROPEAN PHYSICAL JOURNAL A

Regular Article - Theoretical Physics

R-matrix type parametrization of the Jost function for extracting the resonance parameters from scattering data

P. Vaandrager[1,a], **M. L. Lekala**[1], **S. A. Rakityansky**[2,3]

[1] Department of Physics, University of South Africa (UNISA), Pretoria, South Africa
[2] Department of Physics, University of Pretoria, Pretoria, South Africa
[3] Bogolyubov Laboratory of Theoretical Physics, JINR, Dubna, Russia

The method combines the well-known R-matrix approach with the analysis based on the semi-analytic representation of the Jost functions. It is shown that such a combination has the advantages of both these approaches, namely, the number of the fitting parameters remains relatively small (as for the R-matrix approach) and the proper analytic structure of the S-matrix is preserved (as for the Jost function method). It is also shown that the new formalism, although closely related to the R-matrix method, has the benefit of no dependence on an arbitrary channel radius.

$$f_\ell^{(\mathrm{in/out})}(E) = e^{\mp i\delta_\ell^c} k^\ell \left\{ \frac{k}{D_\ell(\eta,k)} A_\ell(E) - [M(k) \pm i]\, D_\ell(\eta,k) B_\ell(E) \right\},$$

$$S(E) = f^{(\mathrm{out})}(E) \left[f^{(\mathrm{in})}(E) \right]^{-1}$$

$$D_\ell(\eta,k) = C_\ell(\eta) k^{\ell+1}, \qquad M(k) = \frac{2\eta h(\eta)}{C_0^2(\eta)},$$

$$h(\eta) = \frac{1}{2}\left[\psi(1+i\eta) + \psi(1-i\eta)\right] - \ln\eta,$$

$$\psi(z) = \frac{\Gamma'(z)}{\Gamma(z)},$$

Resonances are zeros of $f^{(\mathrm{in})}(E)$ at complex E

parametrization

$$A_\ell(E) = \sum_{n=0}^{N} \alpha_{n\ell} \mathscr{P}_n(E) \qquad B_\ell(E) = \sum_{n=0}^{N} \beta_{n\ell} \mathscr{P}_n(E),$$

$$\mathscr{P}_0(E) = \prod_{n=1}^{N} (E_{n\ell} - E),$$

$$\mathscr{P}_n(E) = \frac{\mathscr{P}_0(E)}{E_{n\ell} - E} \qquad \text{for } n > 0.$$

$\alpha_{n\ell}$ and $\beta_{n\ell}$

IOP Publishing

J. Phys. A: Math. Theor. **56** (2023) 315202 (23pp)

Two-fermion lattice Hamiltonian with first and second nearest-neighboring-site interactions

S N Lakaev[1], A K Motovilov[2], S K Abdukhakimov[1]

[1] *Samarkand State University* [2] *JINR Dubna*

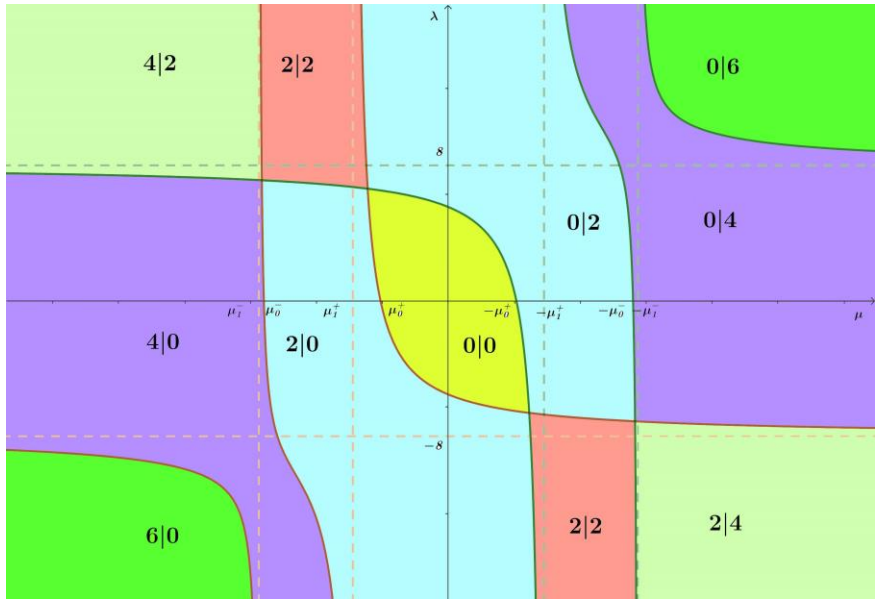

Partition of the (λ, μ)-plane of parameters λ, μ ∈ R in the connected components. These components are tagged by the symbols N_-/N_+ formed of the numbers N_- and N_+ of eigenvalues of the two-fermion Schroedinger operator (corresponding to the zero quasi-momentum of the center of mass) lying below and above the essential spectrum, respectively.

Studied: Hamiltonian H of two identical spinless fermions on the 2D-lattice Z^2,

$$H=H_0+\lambda V_1+\mu V_2, \qquad \lambda, \mu \text{ are real},$$

under an assumption that only the first and second nearest-neighboring-site fermion-fermion interactions V_1 and V_2 are non-zero; λ, μ are the coupling constants. (H_0 denotes the kinetic energy operator.)

First principal result: *A* partition of the (λ, μ) plane is established such that, in each its connected component, the two-fermion Schrödinger operator corresponding to the zero quasi-momentum of the center of mass has definite (fixed) numbers of eigenvalues that are situated below the bottom of the essential spectrum and above its top.

Second principal result: For each connected component, a sharp lower bound is established on the number of isolated eigenvalues for the two-fermion Schrödinger operator corresponding to any admissible nonzero value of the center-of-mass quasimomentum.

``Absence of the three-body bound states for small mass ratio in the two-component system"

Binding of two heavy fermions (of mass m) interacting with a light particle (of mass m_1) via the contact interaction is possible only for sufficiently large heavy-light mass ratio. In this work, the two-variable inequality is derived to determine a specific value μ^* providing that there are no three-body bound states for the mass ratio m/m_1 smaller than μ^*. Namely, the problem reduces to finding the value w^* provided that the condition

$$2\Gamma\left(\frac{L+i\varkappa}{2}+1\right)\Gamma\left(\frac{L-i\varkappa}{2}+1\right)-\varkappa\Gamma\left(\frac{L+i\varkappa+1}{2}\right)\Gamma\left(\frac{L-i\varkappa+1}{2}\right)-\frac{\pi\,2^{1-L}\,(\sin\omega)^L}{\sinh\varkappa\pi\,\cos\omega}\left(\frac{1}{\sin\omega}\,\frac{d}{d\omega}\right)^L\frac{\sinh\varkappa\omega}{\sin\omega}\geq 0$$

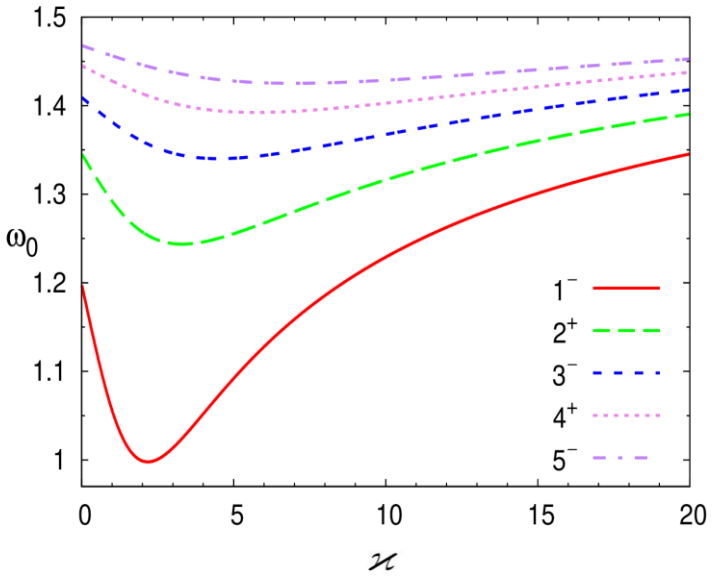

is satisfied for any $0 < w \leq w^* < p/2$ and $\varkappa > 0$, then μ^* follows from the relation $\sin(w^*) = \mu^*/(1+\mu^*)$. In fact, it was proven that minimum of the single-valued function $w_0(\varkappa)$ presented in Figure gives the value $\mu^* = 5.26$ for a total angular momentum and parity $L^P = 1^-$. For other L^P sectors, the specific mass-ratio values providing an absence of the three-body bound states are found in a similar way. For generality, the method is extended so as to determine corresponding mass-ratio values for the system consisting of two identical bosons and a distinct particle for different L^P ($L > 0$) sectors.

The described method will be useful in analytically determining the lower bounds in other three-body problems.

[O.I. Kartavtsev and A.V. Malykh, Eur. Phys. J. Plus 138, 147 (2023)]

Eur. Phys. J. Plus (2024) 139:425

Canal states in bilayer thin films

T P Grozdanov[1], **E A Solov'ev**[2]

[1] *Institute of Physics, Belgrade, Serbia* [2] *JINR Dubna*

Canal states embedded in continuum are studied for a particle interacting with thin of 2D-periodic zero-range potentials in 3D problem. Numerical calculations of canal states are performed for the case of an atomic bilayer on a square lattice. For particle scattering on this system we demonstrate the manifestations of canal states in impact-energy and impact-angles dependence of total reflection/transmission probabilities. Special cases when energy eigenvalues of the canal states tend to scattering thresholds are also analyzed.

Here arises a fundamental aspect of the boundary condition problem in multidimensional case. Where there is a canal states, there simultaneously exist state with incoming plane wave, i.e. they correspond two different type boundary conditions - the boundary condition of the scattering problem and the condition on the bound state along the coordinate perpendicular to the thin film.

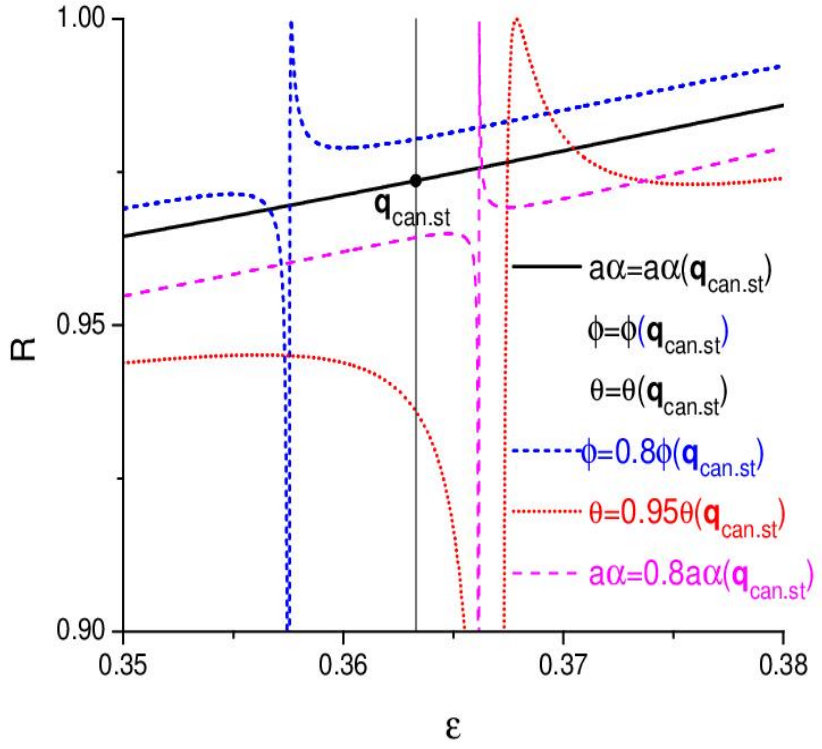

Scattering on the bilayer thin film. The canal state $\mathbf{q}_{can.st.}$ is indicated by the bold black point. The vertical thin line symbolically represents zero-width resonance. This figure demonstrates very unusual behavior. In vicinity of canal state reflectivity has pronounced resonant structure, but at the same parameters as canal state (full black line) it has very smooth behavior as function of impact energy ε without any symptoms of canal state.

Investigation of spectral structure of ^{11}Be in breakup reactions

D.Valiolda, D. Janseitov, V.S. Melezhik,

Chinese Physics C V.49 (5), 2025, https://doi.org/10.1088/1674-1137/adb2fb

Analyzing the calculated breakup cross sections of reactions: ^{11}Be+^{12}C (^{208}Pb)->^{10}Be+n+^{12}C (^{208}Pb) at the same beam energy of 5 MeV/nucleon, it was found two features in the dynamics of the breakup cross section of ^{11}Be: a dramatic increase of the $5/2^+$ resonance at 1.25 MeV and the transformation of the plateau in the 0.3-1.0 MeV region into a broad peak at ~0.3 MeV. The elimination of the excited state ½- from the n-^{10}Be interaction at ^{11}Be+^{12}C ->^{10}Be+n+^{12}C , leads to an increase in the peak at 0.3 MeV, since **the breakup from the ground state ½+ goes directly into the continuous spectrum without intermediate population of the excited state ½-** (Fig.2). A further change in the interaction, leading to in an increase the binding energy of the ground state of ^{11}Be from $E_{1/2+}$=−0.503 MeV, leads to the elimination of the peak and reaching the plateau of the cross section at $E_{1/2+}$≤−1 MeV. **As a result, the presence of the excited state $1/2^-$ decreases its maximum by an order of 35% due to the destructive interference between the transitions $1/2^+ \rightarrow$kf and $1/2^+ \rightarrow 1/2^- \rightarrow$kf .**

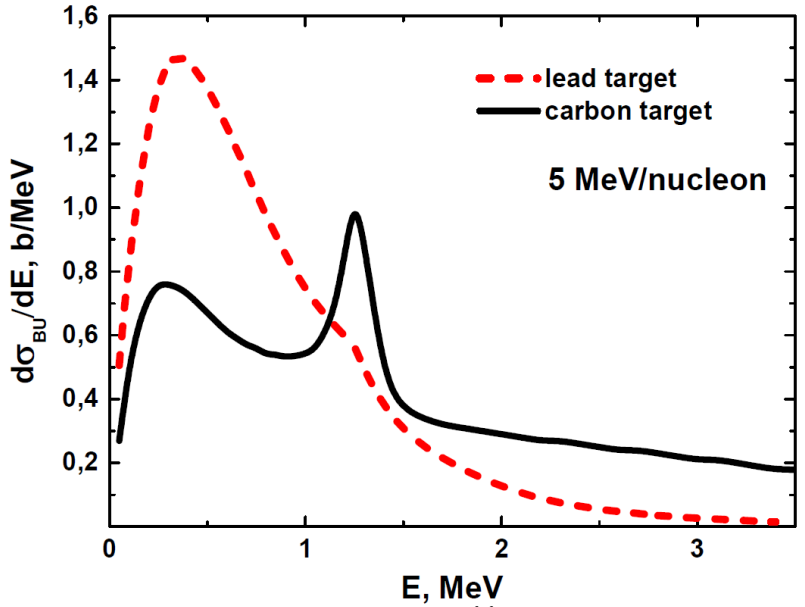

Fig.1. Breakup cross sections of ^{11}Be impinging on light (^{12}C) (x10) and heavy (^{208}Pb) targets at 5 MeV/nucleon calculated within quantum-quasiclassical approach

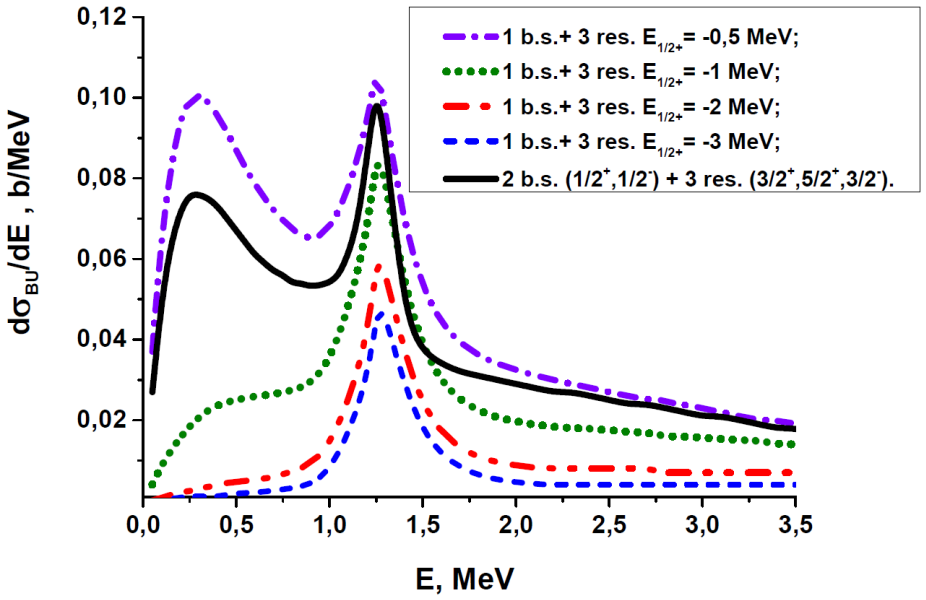

Fig.2. Calculated breakup cross sections of ^{11}Be on ^{12}C with different spectral structure of ^{11}Be-nucleus.

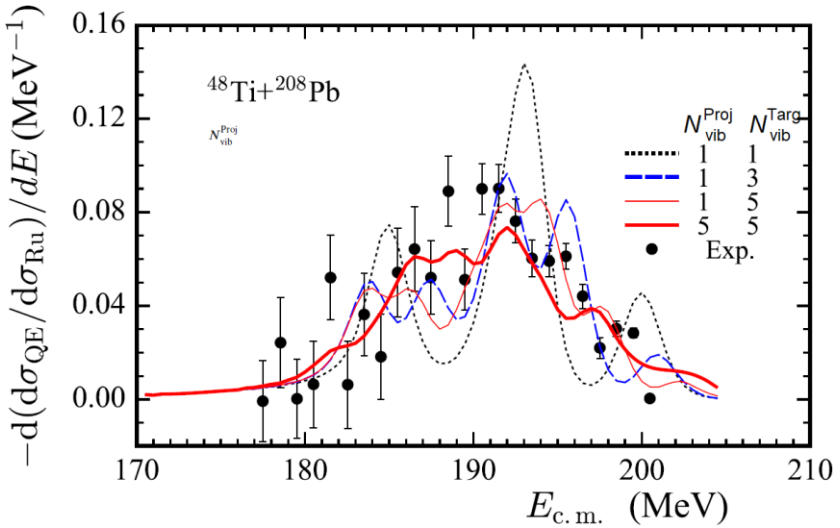

Fig.1. Quasi-Elastic (QE) barrier distributions: the derivative with respect to the collision energy $E_{c.m.}$ of the back-angle QE cross section relative to the Rutherford cross section for reactions ^{48}Ti+^{208}Pb. Experimental data from [S. Mitsuoka, et al, Phys. Rev. Lett. 99 (2007) 182701]. The number of phonons used in vibrational couplings for the projectile and for the target are N_{vib}^{Proj} and N_{vib}^{Targ}. The Coulomb barrier height is 195.40 MeV.

Back-angle quasi-elastic (QE) scattering with optical potential provides critical barrier information in massive nuclear reactions leading to the synthesis of superheavy nuclei. The shapes and peaks of the derivative with respect to the collision energy of the back-angle QE cross section relative to the Rutherford cross section, known as QE barrier distributions, serve as fingerprints of nuclear structures and reaction dynamics. Couplings to collective movements can lead to distinctive peaks in the barrier distributions, but the role of multi-phonon and high-spin states has not been thoroughly investigated.

Using the reactions ^{48}Ti+^{208}Pb and ^{51}V+^{248}Cm with compound nuclei Z=104 and Z=119, as examples, coupled channel (CC) calculations by means of R-matrix method (RM) and the finite element method (FEM), show that account of multi-phonon and high-spin states significantly smooth the barrier distributions, improving the agreement with experimental data. This work can advance the study of superheavy element synthesis by providing reliable barrier information and capture cross sections based on constraints from QE reactions.

Fig. 2. Same as Fig.1 but for ^{51}V + ^{248}Cm. The experimental data from [M. Tanaka, et al, J. Phys. Soc. Jap. 91 (2022) 084201]. The number of excited states included in rotational couplings for the target is N_{rot}^{Targ}. Coulomb barrier height is 225.62 MeV.

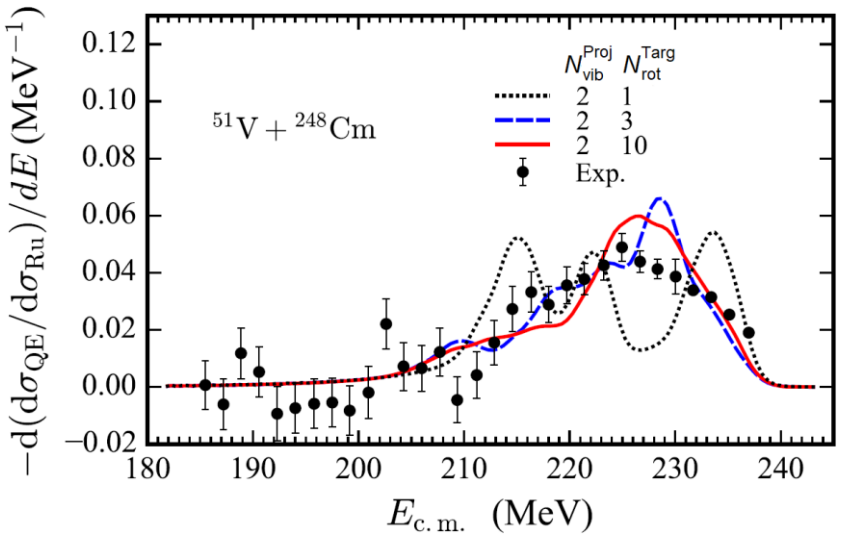

P.W. Wen, O. Chuluunbaatar, P. Descouvemont, A.A. Gusev, C.J.Lin, S.I.Vinitsky, *Role of multi-phonon and high-spin states on the quasi-elastic barrier distributions of massive systems*, Phys. Lett. B 863 (2025) 139383

photonics Photonics **2023**, *10*, 1290. MDPI

Acceleration of Neutral Atoms by Strong Short-Wavelength Short-Range Electromagnetic Pulses

Vladimir S. Melezhik [1,2,*] and Sara Shadmehri [1,*]

[1] Bogoliubov Laboratory of Theoretical Physics, Joint Institute for Nuclear Research, Dubna

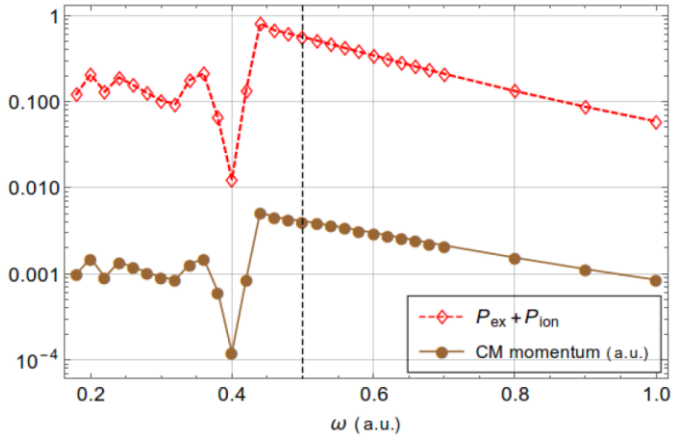

acceleration of neutral atoms due to non-dipole corrections ~ kr=ωy/c in electromagnetic wave E(ωt-kr) and magnetic component E/c in it, leading to non-separability of CM and electron motions, was investigated

Strong correlation was discovered between atom velocity (CM momentum) V_y (MV_y) and total probability of its excitation and ionization $P_{ex}+P_{ion}$

Two resonant mechanisms of atom acceleration established:
through one-photon excitation $V_y \sim I$ (W/cm^2) of atom and
two-photon excitation $V_y \sim I^2$(W/cm^2)

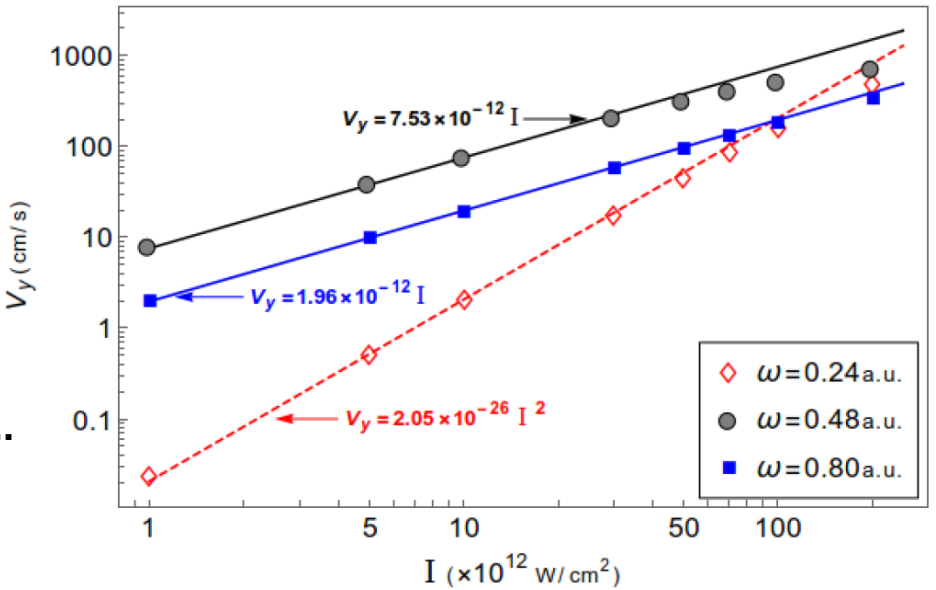

Potential applications: lithography of chips, plazma diagnostic in TOKAMAK ...

E.Kh. Alpomishev, G.G. Adamian, N.V. Antonenko

"Electric conductivity in open quantum two-dimensional nonmagnetic systems: The role of the nondiagonal dissipative kernels and the non-Markovian effect"

Phys. Rev. E112 (2025) 034122

A particularly intriguing subject is the experimental and theoretical study of the properties of two-dimensional (2D) materials in magnetic and electric fields. In many tasks, a 2D material is embedded in an environment that affects its properties.

Using the non-Markovian quantum Langevin approach and taking into account the coupling of charge carriers in 2D nonmagnetic material to the environment and strong correlations between random forces in the x and y components of collective momentum, the analytical expressions have been derived for the transverse component of the electric field and electric conductivity tensor in external stationary and nonstationary electric and nonzero or zero magnetic fields. The role of nondiagonal dissipative kernels and the non-Markovian effect in electric conductivity, orbital diamagnetism, quantum Hall effect and Shubnikovde Haas oscillations is emphasized. The conditions for the dynamic growth of electric conductivity and the magnetic moment are analyzed.

compounds on hydroxylated quartz surfaces from periodic DFT calculations

(Molecular Physics 2025; https://doi.org/10.1080/00268976.2025.2573831)

Valeria Pershina , Miroslav Iliaš

- Adsorption energies (*E*ads) of Lv, Po, and their oxides, hydrides and hydroxides on hydroxylated quartz surfaces are calculated using a periodic DFT
- Elemental Po and Lv should be the most volatile out of all the considered species
- Hydrides of Po and Lv should be less volatile than the elements
- The obtained trend in *E*ads of the Po compounds is in overall agreement with experimental results

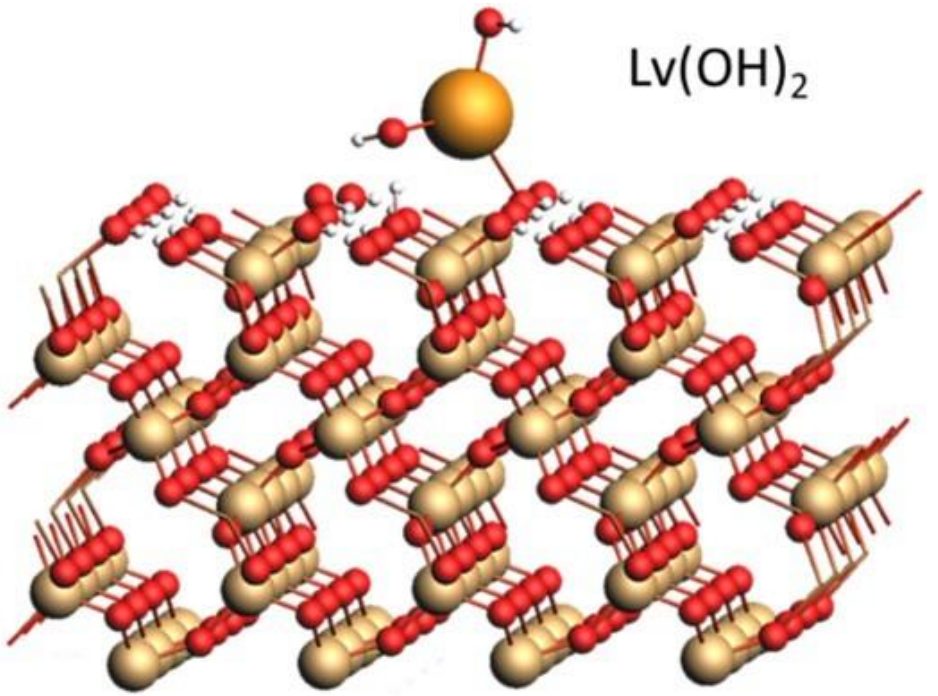

Translationally invariant shell model (TIMO) calculation of the quasielastic (p,2p) process at intermediate relativistic energies

A.B. Larionov, Yu.N. Uzikov, Phys. Rev. C 110 (2024) 1, 014610

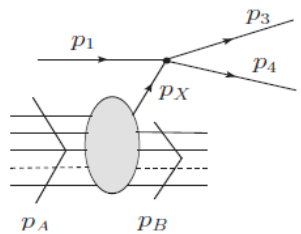

Reaction amplitude (Lorentz invariant by definition) :

Elastic pp amplitude — Spectroscopic amplitude (TIMO)

$$M = M_{\rm el}(p_3,p_4,p_1)A^{1/2}\langle\Psi_B,\psi^{m_l}_{nl}(-\boldsymbol{r})|\Psi_A\rangle\left(\frac{2E_Bm_A}{p^0_X}\right)^{1/2}$$
$$\times\int d^3r e^{-i\boldsymbol{p}_X\boldsymbol{r}}\psi^{m_l}_{nl}(-\boldsymbol{r})F_1(\boldsymbol{r})F_3(\boldsymbol{r})F_4(\boldsymbol{r})\ ,\quad \boldsymbol{r}=\boldsymbol{R}_X-\boldsymbol{R}_B$$

$$F_j(\boldsymbol{r}) = e^{-\frac{\sigma_{NN}(p_j)}{2}\int\limits_{-\infty}^{0}d\eta\,\rho(\boldsymbol{r}\pm\hat{\boldsymbol{p}}_j\eta)}$$

— absorption factors (eikonal), +(-) for incoming (outgoing) particles

p_i – four-momenta,
1 – incoming proton,
A – initial nucleus,
B – final nucleus,
X – struck proton,
3,4 – outgoing protons (in the r.f. of A)

Table 1: Integrated cross sections of the process ^{12}**C**$(p,2p)^{11}$**B with 400 MeV/nucleon ^{12}C beam** for the ground state and two excited states of the residual nucleus ^{11}B. Listed are the results of full calculations (including absorption), calculations in the IA, and the theoretical spectroscopic factors. Experimental data are from Ref. [1]. Total errors are given in parentheses.

E^* (MeV)	J^π	$\sigma_{\rm exp}$ (mb)	$\sigma_{\rm full}$ (mb)	$\sigma_{\rm IA}$ (mb)	S
0.0 (G.S.)	$3/2^-$	15.8(18)	12.3	62.6	2.82
2.12	$1/2^-$	1.9(2)	2.9	14.9	0.67
5.02	$3/2^-$	1.5(2)	3.4	17.5	0.79
Total:		19.2(3)	18.6	95.0	4.28

[1] Data (GSI) ***V. Panin et al., PLB 753, 204 (2016)***

Momentum distribution of the residual nucleus ^{11}B in the r.f. of ^{12}C:

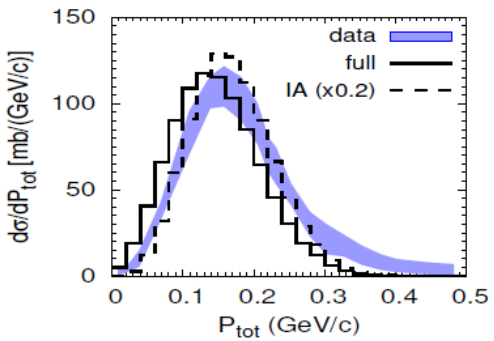

- shift to smaller momenta due to ISI/FSI absorption

- underestimated high-momentum tail (most probably due to HO basis wave functions)

Multiple rescattering effects in the hard knockout reaction ^{2}H(p,2p)n

A.B. Larionov, Eur. Phys. J. A **61** (2025) 160

Метод обобщенного эйконального приближения (GEA) для парциальных амплитуд с двухкратным и трехкратным мягким перерассеянием обобщен на случай произвольных углов вылета протонов в конечном состоянии. Вычислена поправка за счет бесконечного ряда лестничных диаграмм с последовательным перерассеянием протонов. Тем самым уточнён теоретический аппарат для исследования возможных проявлений эффекта цветовой прозрачности в pd столкновениях (см. L.L. Frankfurt, E. Piasetzky, M.M. Sargsian, M.I. Strikman, PRC 56, 2752 (1997); AL, PRC 107 (2023) 014605)

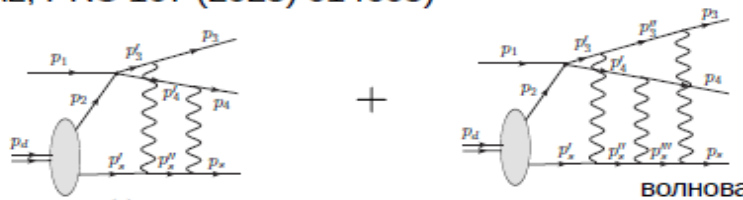

(g)

волновая функция дейтрона , $\boldsymbol{r} = \boldsymbol{r}_2 - \boldsymbol{r}_s$

$$M^{(g)} \equiv M^{(34)} = 2m_N^{1/2} M_{\rm hard} \int d^3r \Theta(-z_3)\Theta(-z_4) \mathrm{e}^{i\boldsymbol{p}_s\boldsymbol{r} - i\Delta_3 z_3 - i\Delta_4 z_4} \phi(\boldsymbol{r}) \Gamma_3(b_3)\Gamma_4(b_4) ,$$

неглауберовские поправки (GEA)

$$\Gamma_j(b_j) \equiv -\frac{i}{4|\boldsymbol{p}_j|m_N} \int \frac{d^2k_t}{(2\pi)^2} \mathrm{e}^{-i\boldsymbol{k}_t\boldsymbol{b}_j} M_{\rm el}(|\boldsymbol{p}_j|, -k_t^2)$$ - профильная функция,

$$\boldsymbol{k}_t \perp \boldsymbol{p}_j, \quad z_j = \boldsymbol{r}\boldsymbol{p}_j/|\boldsymbol{p}_j|, \quad \boldsymbol{b}_j = \boldsymbol{r} - (\boldsymbol{r}\boldsymbol{p}_j)\boldsymbol{p}_j/|\boldsymbol{p}_j|^2, \quad j = 3,4$$

$$\begin{aligned}
\tilde{M}^{(g)} &\equiv M^{(34)} + M^{(343)} + M^{(3434)} + M^{(34343)} + \dots \\
&= 2m_N^{1/2} M_{\rm hard} \int d^3r \Theta(-z_3)\Theta(-z_4)\phi(\boldsymbol{r}) \mathrm{e}^{i(\boldsymbol{p}_s\boldsymbol{r} - \Delta_3 z_3 - \Delta_4 z_4)} \Gamma_3(b_3)\Gamma_4(b_4) \\
&\quad \times [1 - \frac{1}{2}\Gamma_3(b_3) + \frac{1}{4}\Gamma_3(b_3)\Gamma_4(b_4) - \frac{1}{8}\Gamma_3(b_3)\Gamma_4(b_4)\Gamma_3(b_3) + \dots] \\
&= 2m_N^{1/2} M_{\rm hard} \int d^3r \Theta(-z_3)\Theta(-z_4)\phi(\boldsymbol{r}) \mathrm{e}^{i(\boldsymbol{p}_s\boldsymbol{r} - \Delta_3 z_3 - \Delta_4 z_4)} \Gamma_3(b_3)\Gamma_4(b_4) \\
&\quad \times \frac{1 - \Gamma_3(b_3)/2}{1 - \Gamma_3(b_3)\Gamma_4(b_4)/4}
\end{aligned}$$

перенормировочный коэффициент

- Значительная разница между результатами глауберовского расчета и расчета GEA во всех случаях кроме случая покоящегося нейтрона-спектатора.

- Эффект перенормировки за счет множественного перерассеяния значителен, ~50%, в случае вылета нейтрона вперёд (α_s=0.7).

$$t = (p_1 - p_3)^2 = (4m_N^2 - s)/2, \; s = (p_3 + p_4)^2$$

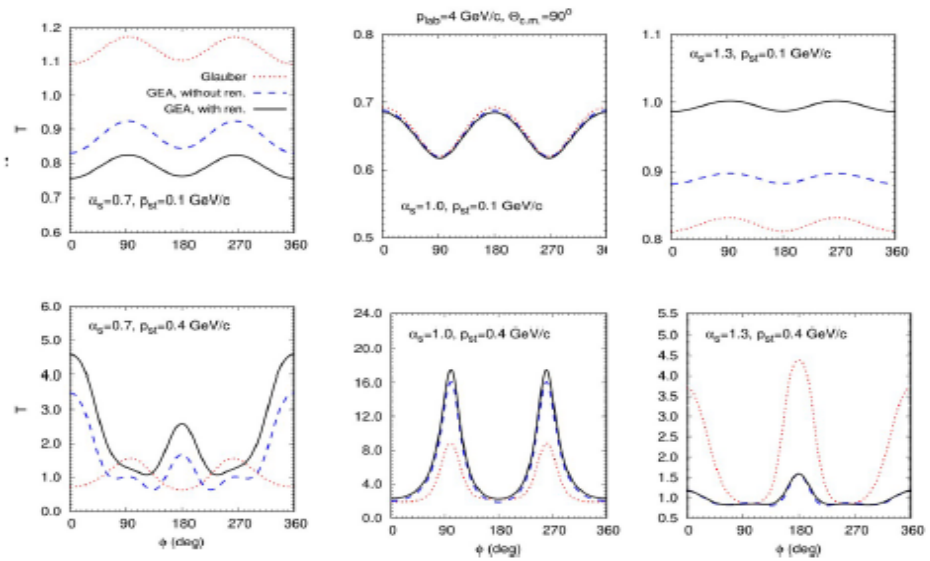

$$T \equiv \frac{\sigma}{\sigma_{\rm IA}}$$ - ядерная прозрачность,

$p_s = (E_s, \boldsymbol{p}_s)$ - 4-импульс нейтрона-спектатора,

$$\alpha_s = \frac{2(E_s - p_s^z)}{m_d}$$ - переменная светового конуса,

$\phi = \phi_3 - \phi_s = \angle(\boldsymbol{p}_{3t}, \boldsymbol{p}_{st})$ - относительный азимутальный угол между рассеянным протоном и нейтроном-спектатором

А.И. Тимов
EPJD 78, 31 (2024)
PEPAN 55, 920 (2024)

Effects of Photon Polarizations in non-linear Compton process

Purpose: Compton photons in electron-laser interactions as a source for high energy photons in e+e- pair production in photon – laser interactions

The energy of the laser photon is an order of one eV, the energy of e+e-pair is > 10^6 eV , therefore the energy of the probe (Compton) photon must be a few dozen of GeV, i. e. ultra-relativistic

The electron in Compton process must be ultra-relativistic!

Previously, we found that the yield of e+e-pair formation depends on the mutual polarization of interacting photons

This year we elaborated a model for the Compton processes as an input for further transport models for e+e- pair production in relativistic electron-laser interactions in a wide region of electron energy and laser beam intensity

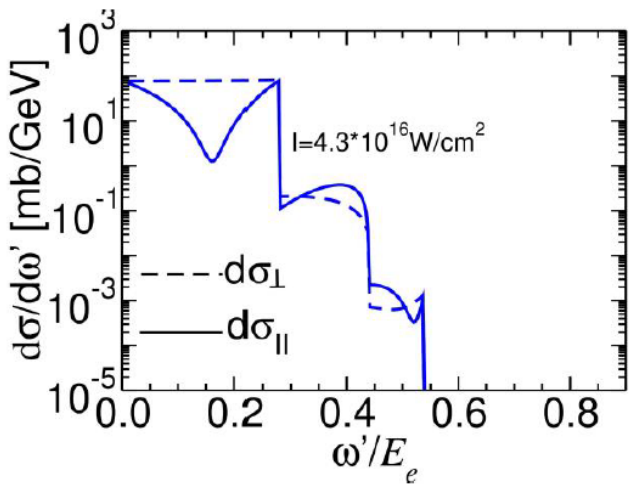

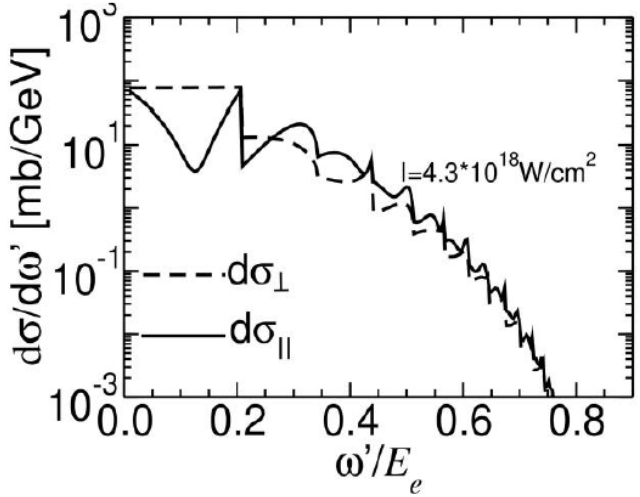

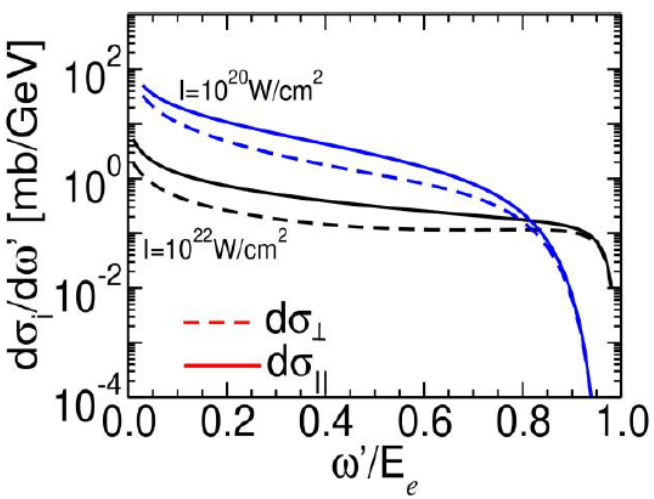

Electron energy $E_e = 16.5\ GeV;$ $\sigma_{\parallel,\perp}$ *for polarization of recoil photon parallel or perpendicular to the laser beam polarization*

ω' *energy of recoil photon*

Analytical calculations of the tenth order QED radiative corrections to lepton anomalies within the Mellin–Barnes representation

O P Solovtsova, V I Lashkevich, and L P Kaptari

Published 28 March 2024 • © 2024 IOP Publishing Ltd

Journal of Physics G: Nuclear and Particle Physics, Volume 51, Number 5, 055001. *Phys.* **51** 055001 **DOI** 10.1088/1361-6471/ad2e32

Corrections up to the tenth order to the anomalous magnetic moment of leptons with various loop inserts of the same leptons are calculated.

A.S. Parvan, *Study on relativistic transformations for thermodynamic quantities: Boltzmann–Gibbs and Tsallis blast-wave models*, **Eur. Phys. J. A 61, 261 (2025)**

Relativistic transformations of thermodynamic quantities $\left(S_0 = S, \quad N_0 = N, \quad V_0 = \gamma V\right)$

Non-Planck transformations	Planck transformations	Ott transformations
$\mathbf{P} = const$	$\mathbf{v} = const$	$\mathbf{v} = const$
$(S, V, N, \mathbf{P})$	$(S, V, N, \mathbf{v})$	$(S, V, N, \mathbf{v})$
$\gamma = \gamma(S, V, N, \mathbf{P})$	$\gamma(\mathbf{v}) = \frac{1}{\sqrt{1-\mathbf{v}^2}}$	$\gamma(\mathbf{v}) = \frac{1}{\sqrt{1-\mathbf{v}^2}}$
$E = \sqrt{\mathbf{P}^2 + E_0^2(S_0, V_0, N_0)}$	$\bar{L} = \frac{E_0(S_0, V_0, N_0)}{\gamma(\mathbf{v})}$	$E = \gamma(\mathbf{v}) E_0(S_0, V_0, N_0)$
$T = \left(\frac{\partial E}{\partial S}\right)_{VN\mathbf{P}} = \frac{\alpha T_0}{\gamma}$	$T = \left(\frac{\partial \bar{L}}{\partial S}\right)_{VN\mathbf{v}} = \frac{T_0}{\gamma}$	$T_* = \left(\frac{\partial E}{\partial S}\right)_{VN\mathbf{v}} = \gamma T_0$
$p = -\left(\frac{\partial E}{\partial V}\right)_{SN\mathbf{P}} = \alpha p_0$	$p = -\left(\frac{\partial \bar{L}}{\partial V}\right)_{SN\mathbf{v}} = p_0$	$p_* = -\left(\frac{\partial E}{\partial V}\right)_{SN\mathbf{v}} = \gamma^2 p_0$
$\mu = \left(\frac{\partial E}{\partial N}\right)_{SV\mathbf{P}} = \frac{\alpha \mu_0}{\gamma}$	$\mu = \left(\frac{\partial \bar{L}}{\partial N}\right)_{SV\mathbf{v}} = \frac{\mu_0}{\gamma}$	$\mu_* = \left(\frac{\partial E}{\partial N}\right)_{SV\mathbf{v}} = \gamma \mu_0$
$E(S,V,N,\mathbf{P})$ - Fundamental thermodynamic potential (Hamiltonian)	$\bar{L}(S,V,N,\mathbf{v})$ - Conjugate fundamental thermodynamic potential (negative Lagrangian)	$E(S,V,N,\mathbf{v})$ - This energy is not a thermodynamic potential

$$\alpha \equiv \frac{1}{1 - \frac{V_0 p_0}{E_0}\frac{\mathbf{P}^2}{E^2}}$$

- ✓ *Planck transformation leads to a consistent pT-distribution*
- ✓ *Ott transformation leads to an inconsistent pT-distribution*

Conferences and Schools

Session-conference of the Nuclear Physics Section, PSD RAS, dedicated to the 70th anniversary of the birth of V.A. Rubakov
Moscow, February 17-21, 2025.

XXX Всероссийская научно-практическая конференция студентов, аспирантов и молодых специалистов
Университет»Дубна», Дубна, Россия, 7 – 11 апреля, 2025

International Conference on Nuclear Structure and Nuclear Reactions,
Aligarh, India, May 5-7, 2025.

International Workshop “Infinite and Finite Nuclear Matter” (INFINUM-2025).
JINR, Dubna, May 12–16, 2025.

The 29th International Nuclear Physics Conference (INPC 2025)
Daejeon, South Korea, May 25–30, 2025.

South Africa-JINR Workshop on Theoretical and Computational Physics:
Dubna, Russia, June 23–27, 2025.

42-th International Workshop on Nuclear Theory:
Rila Mountains, Bulgaria, June 29 – July 5, 2025.



13 KLTP/CAS-BLTP/JINR Joint Workshop on Physics of Strong Interacting Systems,
Almaty, Kazakhstan, 17-22 August, 2025.

LXXV International Conference «NUCLEUS – 2025.
Nuclear physics and elementary particle physics. Nuclear physics technologies
Saint-Petersburg, Russia, July 1 – 6, 2025.

The 50th Vietnam Conference on Theoretical Physics (VCTP-50)
Dalat city, Vietnam, August 4 - 7, 2025.

13 KLTP/CAS-BLTP/JINR Joint Workshop on Physics of Strong Interacting Systems,
Almaty, Kazakhstan, 17-22 August, 2025.

XI International Conference «Modern problems of Nuclear Energy
and Nuclear Technologies»,
Tashkent, October 14-16, 2025

Школа «Современные подходы к созданию детекторных материалов»
НИЦ ``Курчатовский институт",
Москва, Россия, 21-25 октября 2025.

India-JINR Workshop on Particle, Nuclear, Neutrino Physics and Astrophysics,
Bhubaneswar, India, November 10–12, 2025.

The 2025 Asian Nuclear Physics Association (ANPhA) board meeting
& the ANPhA symposium on nuclear physics,
Taipei, 27-29 November 2025.

10th Workshop on the Chemistry of the Heaviest Elements
September 7 – 11, 2025, Dunhuang, China

21 Int. Workshop "Complex Systems of Charged Particles and their Interactions with Electromagnetic Radiation"
April 7 – 11, 2025, Moscow

Thank you for your attention

Grant of the Ministry of Science and Higher Education of the Republic of Kazakhstan

•“Study of the mechanisms of nucleon transfers and the formation of

•neutron-excess isotopes in nuclear reactions with heavy nuclei”

2023-2025 No. AP19577048

Grant from the Russian Science Foundation

"Theoretical study of the synthesis and properties of heavy and superheavy nuclei"

No. 25-42-00018

A.A. Dzhioev, A.V. Yudin, N.V. Dunina-Barkovskaya, A.I. Vdovin, Particles 8 (2025)84

Pre-supernova (anti)neutrino emission due to weak-interaction reactions with hot nuclei

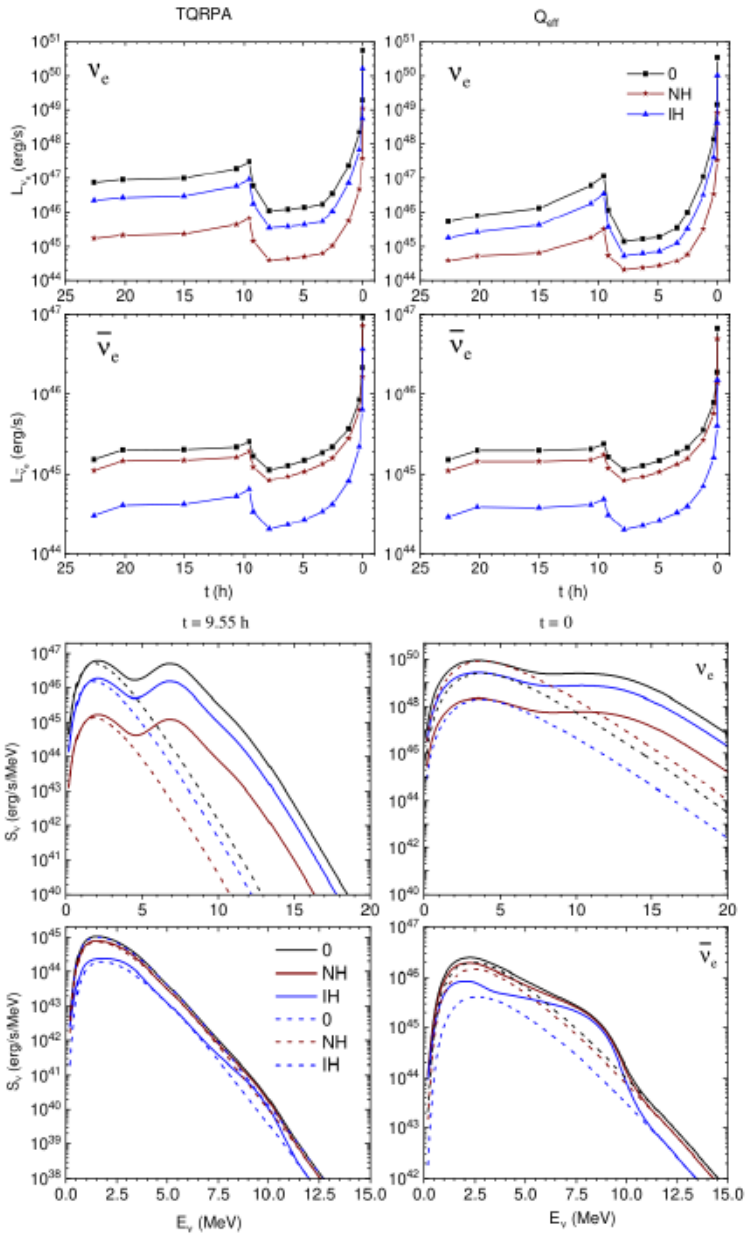

Reliable predictions of (anti)neutrino spectra and luminosities are essential for assessing the feasibility of detecting pre-supernova neutrinos. Using the TQRPA method and the stellar evolution code MESA, we calculate the (anti)neutrino spectra and luminosities under realistic conditions of temperature, density, and electron fraction. Our study includes (anti)neutrinos produced by both thermal processes and nuclear weak-interaction reactions. By comparing the results of the thermal quasiparticle random-phase approximation with the standard technique based on the effective Q-value method, we investigate how thermal effects influence the spectra and luminosities of emitted (anti)neutrinos. Our findings show that a thermodynamically consistent treatment of Gamow–Teller transitions in hot nuclei enhances both the energy luminosity and the average energies of the emitted (anti)neutrinos. As a result, the probability of (anti)neutrino detection by Earth-based detectors increases.

A. Rahmatinejad, T.M. Shneidman, G.G. Adamian, N.V. Antonenko

"Dependence of angular momentum of fission fragments on total kinetic energy in spontaneous fission of ^{252}Cf "

Phys. Rev. C112, 044610 (2025)

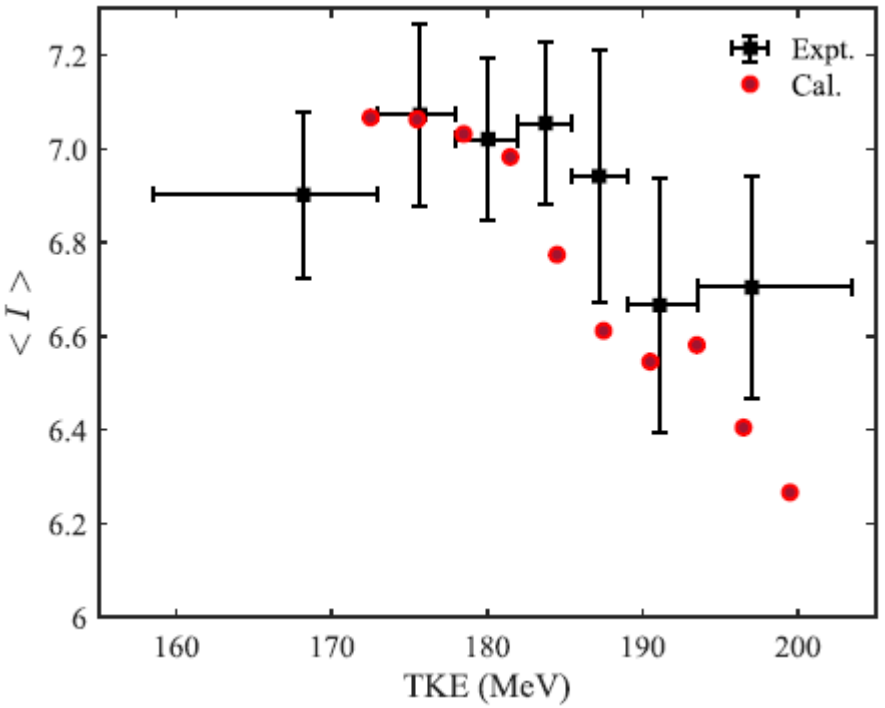

Average angular momentum $< I >$ of postscission ^{144}Ba as a function of total kinetic energy
Calculations - red circles
Experiment - black squares

A weak dependence of the angular momentum of ^{144}Ba fragments, produced in spontaneous fission of ^{252}Cf, on total kinetic energy (TKE) was observed.

Model was developed to explain phenomenon. It assumes: after tunneling through fission barrier, the nucleus can be represented by a superposition of dinuclear systems (DNS). The angular motion in the DNS is treated quantum-mechanically, yielding the angular momentum distribution of nuclei at scission configurations leading to ^{144}Ba fragments. Within this framework, experimentally observed dependence of the average angular momentum of ^{144}Ba on TKE was successfully reproduced.

B. Urazbekov, N. Burtebayev, **D. Janseitov**, M. Nassurlla, **D. Valiolda**, D. Alimov. Examination of collective and single-particle models for excited states of ^{13}C below 10 MeV in nuclear reactions induced by 18 MeV deuteron beam" // Eur. Phys. J. A 60, 86 (2024).

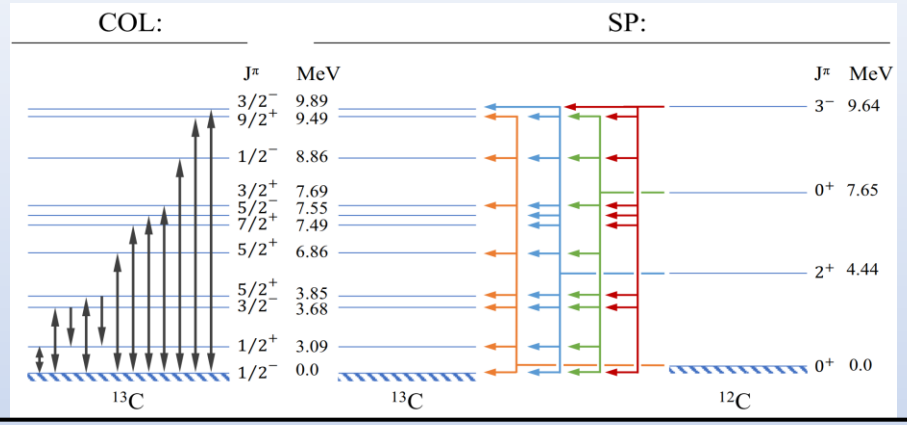

Coupling schemes for both the collective (COL) and single-particle (SP) models used in the CC calculation. Excited states for the ^{13}C nucleus are given up to 10 MeV

This paper presents a study of both the elastic and inelastic scattering of a deuteron beam on ^{13}C at laboratory energy of 18 MeV.

Experiment: the cyclotron U-150M at the Institute of Nuclear Physics in Almaty, the Republic of Kazakhstan.

Research methods: various theoretical models, such as: optical, folding and the coupled channels methods.

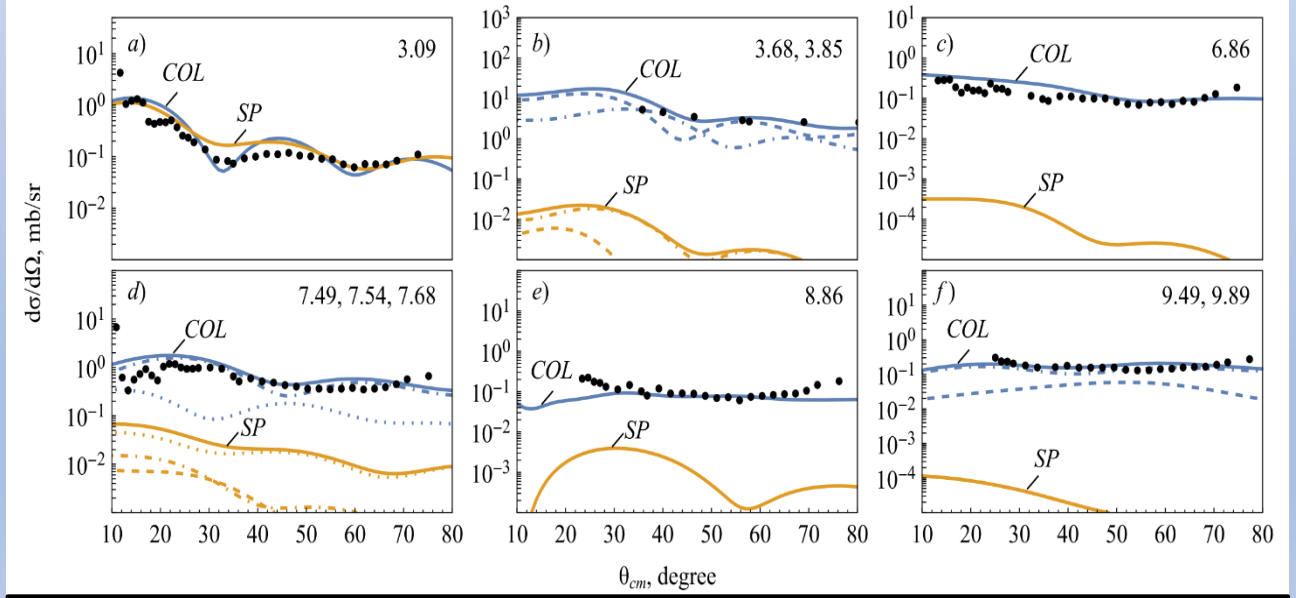

CC calculations performed on one-particle (SP, yellow line) and collective (Col,blue line) models of $^{13}C(d,d)^{13}C$ with differential cross-section data of inelastic scattering channels.

The paper provides an analysis of data on the angular distribution of both the elastic and inelastic channels after the d+^{13}C nuclear reaction at laboratory energy of 18 MeV. ***Elastic scattering*** data were taken into account in analyzing the ***optical model***, and ***inelastic channels*** were taken into account in the ***coupled channel method***. In the inelastic channels, the target nucleus was modeled as having ***single-particle and collective modes***. The semi-microscopic ***double-folding potential*** was obtained and its applicability was shown to describe both elastic and inelastic channels. **The ability of the collective model to describe all excited states was demonstrated by good agreement when comparing the calculated cross sections in the collective model and experimental data. The single-particle model turned out to be significant only for the excited state of 3.09 MeV.**

Jolos R.V., Kolganova E.A. *Pseudospin Symmetry and Quasidouble Magic Nuclei //* Eur. Phys. J. A. 2025. V. 61. P. 115. URL: https://doi.org/10.1140/epja/s10050-025-01595-5.

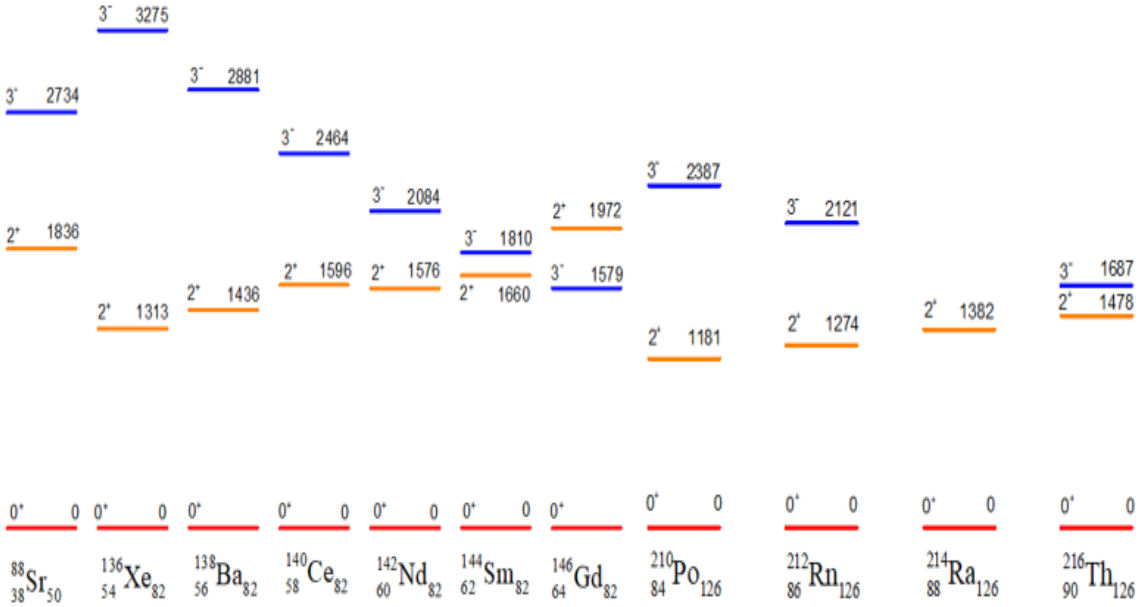

Evolution of excitation energies of the low-lying 2^+ and 3^- states (in keV) in semimagic nuclei.

Эволюция энергий возбуждения нижайших 2^+ и 3^- состояний (в кэВ) в ядрах, близких к квазимагическим

The similarities in the properties of the nuclei with neutron closed shell and with protons filling valence shell are considered. It is shown that the available experimental data or calculations demonstrate the existence of two regions of nuclei, namely, with Z = 29 - 38, N = 50; Z = 51 − 64, N = 82 and Z = 83 - 100, N = 126, whose properties indicate on similarity with nuclei in the environment of the quasidouble magic ^{146}Gd. The reason for this is that the proton single-particle levels filling the regions under consideration form a pseudospin doublets.

Проведен анализ структуры ядер с Z = 29−38 и N = 50, Z = 51−64 и N = 82, а также Z = 83 − 100 и N = 126, в которых нейтронная оболочка уже заполнена, а протоны только начинают заполнять валентную оболочку. Обнаружено, что нижние одночастичные уровни в протонной оболочке существенно отделены от остальных уровней этой оболочки и образуют псевдоспиновые дублеты. Показано, что причиной их отделения от остальных уровней той же оболочки является большая величина расщепления по псевдоорбитальному моменту. Такие ядра приобретают ряд свойств, делающих их похожими на дважды магические ядра.

J. Chem. Phys. 162, 174304 (2025); doi: 10.1063/5.0263618

Acceleration and twisting of neutral atoms by strong elliptically polarized short-wavelength laser pulses

Vladimir S. Melezhik[1,2,a)] and Sara Shadmehri[3,b)]

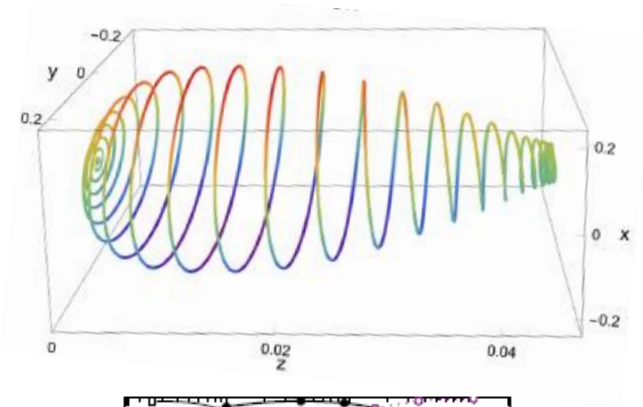

An m-photon resonance mechanism has been proposed and investigated for the twisting of atoms by a circularly polarized laser pulse (with the frequency of mω)

$$H_{n=1} + m(\hbar\omega) \rightarrow H_{n'} \ , \ \ m(\hbar\omega) = \frac{1}{2n} - \frac{1}{2n'}$$

with the transfer of photon helicity to them .
As a result of interaction with the laser, the atom accelerates/decelerates and twists – it acquires orbital momentum with a projection of L_z=mħ on the direction of it motion oZ.

The proposed alternative for twisting atoms opens up new possibilities compared to the technique using fork-shaped diffraction gratings, which was developed for twisting elementary particles (photons and electrons), but is unsuitable for composite particles (protons, neutrons, and atoms).

Indeed, despite a 30-year history of experimental research on twisted photons and electrons, producing twisted atoms remains a highly complex experimental task. Despite numerous attempts, only one experiment has been completed to date on twisting helium atoms using a special fork-shaped diffraction grating

A. Luski et. al., Science **373**, 1105 (2021)

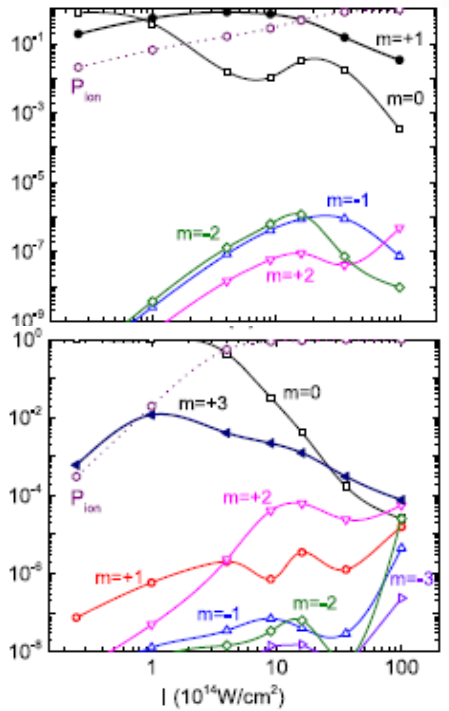

Populations $P_m(I)$ of the projections of the orbital momentum **m** on oZ-axis and the ionization probability $P_{ion}(I)$ of the atom at the end of an 8fs-laser pulse of intensity I for two resonant frequencies ω (top) and ω′(bottom) : ħω=3ħω′ = 0.48a.u.